Representing the Dynamic Response of Vegetation to Nitrogen Limitation in the CLASSIC Land Model

Sian Kou-Giesbrecht[1] and Vivek Arora[1]

[1]Canadian Centre for Climate Modelling and Analysis

November 22, 2022

Abstract

Despite its pivotal feedback to carbon cycling, representing the dynamic response of vegetation to nitrogen limitation is a key challenge for simulating the terrestrial carbon sink in land models. Here, we explore a representation of this dynamic response of vegetation to nitrogen limitation with a novel representation of biological nitrogen fixation and nitrogen cycling in the Canadian Land Surface Scheme Including Biogeochemical Cycles (CLASSIC) model. First, we assess how incorporating this dynamic response of vegetation to nitrogen limitation via biological nitrogen fixation influences carbon sequestration for CO_2 and nitrogen fertilisation experiments, comparing simulations against observation-based estimates from meta-analyses. This evaluates whether underlying mechanisms are realistically represented. Second, we assess how incorporating the dynamic response of vegetation to nitrogen limitation via biological nitrogen fixation affects carbon sequestration over the late 20th and early 21st century, examining the effects of global change drivers (CO_2, nitrogen deposition, climate, and land use change) acting both individually and concurrently. Including nitrogen cycling reduces the terrestrial carbon sink driven by elevated atmospheric CO_2 concentration over the historical period. Representing the dynamic response of vegetation to nitrogen limitation via biological nitrogen fixation increases the present-day terrestrial carbon sink by 0.2 Pg C yr^{-1} because the upregulation of biological nitrogen fixation driven by stronger nitrogen limitation under elevated atmospheric CO_2 concentration alleviates nitrogen limitation. Our results highlight the importance of the dynamic response of vegetation to nitrogen limitation for realistically projecting the future terrestrial carbon sink under global change with land models.

Hosted file

`classic_bnf_si.docx` available at https://authorea.com/users/540098/articles/600120-representing-the-dynamic-response-of-vegetation-to-nitrogen-limitation-in-the-classic-land-model

Representing the Dynamic Response of Vegetation to Nitrogen Limitation in the CLASSIC Land Model

Sian Kou-Giesbrecht[1]* and Vivek K. Arora[1]

[1]Canadian Centre for Climate Modelling and Analysis, Environment and Climate Change Canada, Victoria, B.C., Canada.

Corresponding author: Sian Kou-Giesbrecht (sian.kougiesbrecht@ec.gc.ca)

Key Points:

- The dynamic response of vegetation to nitrogen limitation is critical for projecting the terrestrial carbon sink with land models

- Upregulated biological nitrogen fixation driven by stronger nitrogen limitation under elevated CO_2 alleviates nitrogen limitation

- This determines the response of terrestrial carbon and nitrogen cycling to CO_2, nitrogen deposition, and other global change drivers

Abstract

Despite its pivotal feedback to carbon cycling, representing the dynamic response of vegetation to nitrogen limitation is a key challenge for simulating the terrestrial carbon sink in land models. Here, we explore a representation of this dynamic response of vegetation to nitrogen limitation with a novel representation of biological nitrogen fixation and nitrogen cycling in the Canadian Land Surface Scheme Including Biogeochemical Cycles (CLASSIC) model. First, we assess how incorporating this dynamic response of vegetation to nitrogen limitation via biological nitrogen fixation influences carbon sequestration for CO_2 and nitrogen fertilisation experiments, comparing simulations against observation-based estimates from meta-analyses. This evaluates whether underlying mechanisms are realistically represented. Second, we assess how incorporating the dynamic response of vegetation to nitrogen limitation via biological nitrogen fixation affects carbon sequestration over the late 20th and early 21st century, examining the effects of global change drivers (CO_2, nitrogen deposition, climate, and land use change) acting both individually and concurrently. Including nitrogen cycling reduces the terrestrial carbon sink driven by elevated atmospheric CO_2 concentration over the historical period. Representing the dynamic response of vegetation to nitrogen limitation via biological nitrogen fixation increases the present-day terrestrial carbon sink by 0.2 Pg C yr^{-1} because the upregulation of biological nitrogen fixation driven by stronger nitrogen limitation under elevated atmospheric CO_2 concentration alleviates nitrogen limitation. Our results highlight the importance of the dynamic response of vegetation to nitrogen limitation for realistically projecting the future terrestrial carbon sink under global change with land models.

1 Introduction

Terrestrial ecosystems sequester approximately a quarter of anthropogenic CO_2 emissions (Friedlingstein et al., 2019; Le Quéré et al., 2018). However, the persistence of the terrestrial carbon (C) sink is dependent on the availability of nitrogen (N), which is an essential limiting nutrient to plant growth across terrestrial ecosystems (Elser et al., 2007; LeBauer & Treseder, 2008; Wright et al., 2018). Land models are widely applied within the framework of Earth System Models to simulate the terrestrial C sink and inform climate change mitigation policy (Arora et al., 2020). Coupled C and N cycling is a recent progression in land models and there are a multitude of uncertainties in its representation due to the complexity of terrestrial N cycle processes (Davies-Barnard et al., 2020). As a result, the influence of N limitation of plant growth on the terrestrial C sink remains uncertain in land models (Thomas et al., 2015).

A key challenge is representing the capacity of vegetation to dynamically respond to N limitation. In particular, the representation of biological N fixation (BNF), which is the conversion of atmospheric nitrogen gas (N_2) to a plant-available form of N by bacteria, is a central focus (Meyerholt et al., 2020; Peng et al., 2020; Stocker et al., 2016; Thomas et al., 2015; Wieder et al., 2015). BNF is the primary natural input of N to terrestrial ecosystems (Fowler et al., 2013; Vitousek et al., 2013). Symbiotic BNF, which occurs via symbioses between plants and N-fixing bacteria occupying plant root nodules, can respond dynamically to N limitation: plants can upregulate and downregulate symbiotic BNF when N-limited and non-N limited respectively (Menge et al., 2015). Most C-N coupled land models represent BNF phenomenologically using the empirical relationship of BNF with either net primary production or evapotranspiration (Davies-Barnard et al., 2020), which cannot represent the regulation of BNF by N limitation. A small number of recent C-N coupled land models incorporate a

58 mechanistic BNF representation, in which C allocation to symbiotic BNF is optimized to
59 maximize plant growth, capturing the dynamic response of symbiotic BNF to N limitation, such
60 as CABLE (Haverd et al., 2018; Peng et al., 2020; Wang et al., 2010), CLM5 (Lawrence et al.,
61 2019), E3SM (Zhu et al., 2019), GFDL LM3-SNAP (Kou-Giesbrecht et al., 2021; Sulman et al.,
62 2019), and O-CN (Meyerholt et al., 2020). In addition to regulating symbiotic BNF, plants can
63 respond dynamically to N limitation by increasing C:N ratios (Elser et al., 2010; Meyerholt &
64 Zaehle, 2015; Sistla & Schimel, 2012), by allocating C to mycorrhizae which secrete enzymes
65 that accelerate the decomposition of soil organic matter (Phillips et al., 2013), and rhizosphere
66 priming (primarily through root C exudation which stimulates the decomposition of soil organic
67 matter; Cheng et al., 2014; Finzi et al., 2015), among others. These strategies modulate the extent
68 to which N limitation constrains terrestrial C sequestration and their representation in land
69 models would enable more realistic projections of the terrestrial C sink.

70   Global change drivers influence N limitation of plant growth and consequently
71 representing the dynamic response of vegetation to N limitation is necessary to simulate the
72 terrestrial C sink under global change. As the dominant natural input of N to terrestrial
73 ecosystems, BNF plays an important role in regulating the response of vegetation to global
74 change drivers (Terrer et al., 2018; Zheng et al., 2019, 2020): Symbiotic BNF has been observed
75 to increase in response to elevated atmospheric CO_2 concentration (which intensifies N limitation
76 ; Luo et al., 2004; Terrer et al., 2019) but decrease in response to elevated N deposition (which
77 relieves N limitation ; Zheng et al., 2019, 2020). As global change drivers interact and amplify,
78 projecting the terrestrial C sink under future global change requires a representation of the
79 dynamic response of vegetation to N limitation in land models.

80   Here we present an analysis of terrestrial C and N cycling as regulated by the dynamic
81 response of vegetation to N limitation over the historical period. We include a novel
82 representation of BNF in the Canadian Land Surface Scheme Including Biogeochemical Cycles
83 (CLASSIC) model (Melton et al., 2020; Seiler et al., 2021), which is the land component in the
84 family of the Canadian Earth System Models (CanESM; Arora et al., 2009; Swart et al., 2019).
85 CLASSIC recently adopted a representation of N cycling (Asaadi & Arora, 2021). We improve
86 the previous static representation of BNF that is unresponsive to N limitation by implementing a
87 representation of symbiotic BNF that is regulated by N limitation and thus responds to elevated
88 atmospheric CO_2 concentration and elevated N deposition. In addition, we implement an
89 independent representation of free-living BNF. We use CLASSIC to address the following
90 questions: How do experimental manipulations of global change drivers (specifically, elevated
91 CO_2 and N fertilisation) influence N limitation of plant growth, symbiotic BNF, and the dynamic
92 response of vegetation to N limitation in comparison to observation-based estimates from meta-
93 analyses? How have global change drivers (i.e., atmospheric CO_2 concentration, N deposition,
94 climate, and land use change) over the historical period, individually and concurrently,
95 influenced the dynamic response of vegetation to N limitation and the terrestrial C sink?

2 CLASSIC model structure and C-N cycle interactions

97   CLASSIC simulates land-atmosphere fluxes of energy, momentum, water, C, and N, and
98 it can be run at a point, regional or global scale and at any spatial resolution. Here, a spatial
99 resolution of 2.81˚C is used. A brief overview of physical processes and C biogeochemical
100 processes in CLASSIC is provided in Section 2.1, and is described in detail in Melton et al.,
101 2020; Seiler et al., 2021. An overview of N biogeochemical processes in CLASSIC is provided

102   in Section 2.2. These are described in detail in Asaadi & Arora, 2021. The new representation of
103   the dynamic response of vegetation to N limitation of plant growth in CLASSIC, including BNF,
104   is introduced in Section 2.3.

105   2.1 Overview of CLASSIC

106   2.1.1 Physical processes

107   The physical component of CLASSIC simulates fluxes of energy, momentum, and water
108   at a 30 minute time step and evolved from the Canadian Land Surface Scheme (CLASS;
109   Verseghy, 1991; Verseghy et al., 1993). The soil profile is represented by 20 soil layers, starting
110   with 10 soil layers of 0.1 m thickness followed by soil layers of increasing thickness up to a soil
111   layer of 30 m thickness for a total depth of over 61 m. The depth of permeable soil layers and
112   thus the depth to bedrock soil layers varies geographically and is specified based on the
113   SoilGrids250m data set (Hengl et al., 2017). Each grid cell is considered independent and there
114   are no lateral transfers of energy, momentum, and water between grid cells.

115   2.1.2 Carbon biogeochemical processes

116   The biogeochemical component of CLASSIC simulates the land-atmosphere exchange of
117   C via photosynthesis, autotrophic respiration and heterotrophic respiration, land use change, and
118   fire and evolved from the Canadian Terrestrial Ecosystem Model (CTEM; Arora & Boer,
119   2005a). CLASSIC's photosynthesis equations are based on the standard biochemical model of
120   photosynthesis in Collatz et al., 1991, 1992; Farquhar et al., 1980. Photosynthesis is simulated at
121   a 30 minute time step similarly to the physical component of CLASSIC while all other
122   biogeochemical processes are simulated at a daily time step. For biogeochemical processes,
123   vegetation is partitioned into nine PFTs: needleleaf evergreen trees, needleleaf deciduous trees,
124   broadleaf evergreen trees, broadleaf cold deciduous trees, broadleaf drought deciduous trees, C_3
125   crops, C_4 crops, C_3 grasses, and C_4 grasses. Figure S1 is a schematic illustration of the structure
126   of the biogeochemical component of CLASSIC.

127   CLASSIC prognostically simulates the C pool in vegetation, litter, and soil organic
128   matter for each PFT and over the bare soil fraction in each grid cell. Vegetation C is represented
129   by three C pools: leaf, stem, and root (C_L, C_S, and C_R, respectively; kg C m^{-2}), each of which
130   consists of structural and non-structural C pools. Litter and soil organic matter are represented by
131   the litter C pool (C_D; kg C m^{-2}) and the soil organic C pool (C_H; kg C m^{-2}) respectively.

132   Photosynthesis generates non-structural carbohydrates which are allocated between the
133   non-structural leaf, stem, and root C pools. Autotrophic respiration occurs from the non-
134   structural leaf, stem, and root C pools (Arora & Boer, 2005a). Non-structural carbohydrates are
135   converted to structural carbohydrates as C is transferred from the non-structural C pools to the
136   structural C pools for each vegetation component (Asaadi et al., 2018).

137   Leaf, stem, and root turnover transfer C from the vegetation C pool to the to the litter C
138   pool. In addition to normal leaf turnover, leaf turnover also occurs due to drought stress, cold
139   stress, and shorter day lengths, affecting leaf phenology (Arora & Boer, 2005a). Land use change
140   transfers C from the vegetation C pool to the litter C pool as well as the vegetation product pools,
141   whereas fire emits C to the atmosphere and also transfers C from the vegetation C pool to the
142   litter C pool (Arora & Boer, 2005b, 2010; Arora & Melton, 2018). C associated with

143   decomposing litter is transferred from the litter to the soil organic C pool. Finally, heterotrophic
144   respiration occurs from both the litter and soil organic C pools (Melton et al., 2015).

145   2.2 Nitrogen biogeochemical processes in CLASSIC

146   CLASSIC simulates the land-atmosphere exchange of N via BNF (free-living and
147   symbiotic), specified atmospheric N deposition and N fertiliser application, nitric oxide (NO)
148   emissions, nitrous oxide (N_2O) emissions, N_2 emissions, ammonia (NH_3) volatilisation, N
149   leaching, and land use change (Asaadi & Arora, 2021). Similar to C cycling, CLASSIC
150   prognostically simulates the N pool in vegetation, litter, soil organic matter, and inorganic soil N
151   for each PFT and over the bare soil fraction in each grid cell. Vegetation N is represented by
152   three N pools: leaf, stem, and root (N_L, N_S, and N_R, respectively; g N m^{-2}), each of which
153   consists of structural and non-structural N pools. Litter and soil organic matter are represented by
154   the litter N pool (N_D; g N m^{-2}) and the soil organic N pool (N_H; g N m^{-2}). Inorganic soil N is
155   represented by the soil NH_4^+ pool (N_{NH_4}; g N m^{-2}), and the soil NO_3^- pool (N_{NO_3}; g N m^{-2}). N
156   budget equations are described Text S1. Parameter values for new parameterisations are given in
157   Table S1.

158   N enters the soil-vegetation system via BNF, atmospheric N deposition, and N fertiliser
159   application. Atmospheric N deposition and N fertiliser application enter the soil NH_4^+ and NO_3^-
160   pools. In the previous static representation of BNF in CLASSIC, BNF was not separated into its
161   free-living and symbiotic components – it was represented as a function of soil temperature and
162   soil moisture that contributed to the soil NH_4^+ pool (Asaadi & Arora, 2021). In the new dynamic
163   representation of BNF in CLASSIC presented here, free-living and symbiotic BNF are calculated
164   separately. Free-living BNF contributes to the soil organic N pool and symbiotic BNF
165   contributes to the vegetation N pool. Root uptake of the soil NH_4^+ and NO_3^- pools occurs through
166   both the passive and active pathway. Together, root uptake of the soil NH_4^+ and NO_3^- pools and
167   symbiotic BNF are allocated between the non-structural leaf, stem, and root N pools. Similar to
168   C cycling, N is moved from the non-structural N pools to the structural N pools for each
169   vegetation component.

170   N demand of a given vegetation component is determined based on the fraction of net
171   primary productivity (NPP) allocated to that vegetation component divided by the minimum
172   prescribed C:N ratio for that vegetation component:

173    $$\Delta_i = \frac{\max(0, \alpha_i NPP)}{C:N_{i,min}}, i = L, S, R \tag{1}$$

174   where Δ_i is N demand of vegetation component i (g N m^{-2} day^{-1}), NPP is net primary
175   productivity (kg C m^{-2} day^{-1}), α_i is the fraction of NPP allocated to vegetation component i
176   (unitless), and $C:N_{i,min}$ is the minimum prescribed C:N ratio for vegetation component i (kg C g
177   N^{-1}). This assumes that vegetation attempts to achieve the minimum prescribed C:N ratio for all
178   vegetation components. N demand of vegetation (Δ_V; g N m^{-2} day^{-1}) is the sum of the N demand
179   of its components:

180    $$\Delta_V = \Delta_L + \Delta_S + \Delta_R \tag{2}$$

181   N allocation to a given vegetation component depends both on plant uptake of N and the
182   N demand of that vegetation component:

183
$$A_i = \begin{cases} \frac{\Delta_i}{\Delta_V}(U + B_s) & NPP > 0 \\ \frac{1/C:N_{i,min}}{\Sigma_i 1/C:N_{i,min}}(U + B_s) & NPP \le 0 \end{cases}, i = L, S, R \qquad (3)$$

184 where A_i is N allocation to vegetation component i (g N m^{-2} day^{-1}), U is root uptake of soil NH$_4^+$
185 and NO$_3^-$ through both the passive and active pathway (g N m^{-2} day^{-1}) and B_s is symbiotic BNF
186 (g N m^{-2} day^{-1}). When NPP is negative, such as for broadleaf cold deciduous trees during the
187 winter, N allocation to a given vegetation component is determined based on its prescribed
188 minimum C:N ratio. Because the C and N pools of each vegetation component are determined
189 prognostically and independently, the C:N ratios for each vegetation component and thus the
190 C:N ratio for vegetation evolve freely.

191   N processes associated with turnover and land use change follow the corresponding C
192 processes. Leaf, stem, and root turnover transfer N from the vegetation N pool to the litter N
193 pool. Land use change also transfers N from the vegetation N pool to the litter N pool, vegetation
194 product pools, and atmosphere. N associated with decomposing litter is transferred from the litter
195 to the soil organic N pool. The litter C:N ratio evolves freely driven by the C:N ratio for
196 vegetation components. N mineralisation occurs from both the litter and soil matter N pools and
197 contributes to the NH$_4^+$ pool. Opposing N mineralisation, N immobilization occurs from the
198 NH$_4^+$ and NO$_3^-$ pools and contributes to the soil organic N pool to maintain a prescribed C:N
199 ratio of 13. Soil organic matter is the only pool in CLASSIC with a constant C:N ratio.
200 Nitrification transfers N from the NH$_4^+$ pool to the NO$_3^-$ pool and emits NO and N$_2$O.
201 Denitrification transfers N from the NO$_3^-$ pool to the atmosphere as N$_2$ and emits NO and N$_2$O as
202 well. NH$_3$ volatilization transfers N from the NH$_4^+$ pool to the atmosphere as NH$_3$. N is leached
203 from the NO$_3^-$ pool.

204   Free-living BNF is represented as a function of temperature and soil organic C (which
205 serves as a proxy for microbial biomass):

206        $$B_f = r_{BNF,f} f(\overline{T_k}) C_H \qquad (4)$$

207 $r_{BNF,f}$ is a rate parameter for free-living BNF (g N kg C^{-1} day^{-1}), $f(\overline{T_k}) = \exp\left(-2.6 + \right.$

208 $\left. 0.21\overline{T_k}\left(1 - \frac{0.5\overline{T_k}}{24.4}\right)\right)$ is the temperature dependence function from Houlton et al., 2008 (unitless),

209 where $\overline{T_k}$ is average soil temperature across the soil layers in the top 50 cm (in which free-living
210 BNF is assumed to occur) (°C). Note that free-living BNF can also occur in other ecosystem
211 niches, such as in bryophytes and lichens (Reed et al., 2011), which are not represented.

212   2.3 Dynamic response of vegetation to nitrogen limitation of plant growth in CLASSIC

213   Vegetation exhibits a dynamic response to N limitation of plant growth via three
214 strategies in CLASSIC. First, vegetation upregulates and downregulates symbiotic BNF in
215 response to weak N limitation and strong weak N limitation respectively. Second, vegetation
216 modulates the C:N ratios for each vegetation component and thus the C:N ratio of vegetation in
217 response to changing C and N supply. Finally, photosynthesis carboxylation capacity is
218 dependent on leaf N such that, when leaf N is low, photosynthetic capacity is downregulated and,
219 when leaf N is high, photosynthetic capacity is upregulated.

220   2.3.1 Symbiotic BNF

221   Symbiotic BNF is represented as a function of temperature and N stress of vegetation:

222 $$B_s = r_{BNF,s} \max\left(0, N_{stress} - b_{BNF,s}\right) f(T) \tag{5}$$

223 B_s is symbiotic BNF (g N m^{-2} day^{-1}), N_{stress} is N stress of vegetation (unitless, varies between 0
224 and 1), $r_{BNF,s}$ is a PFT-dependent BNF rate (g N m^{-2} day^{-1}), and $b_{BNF,s}$ is a parameter describing
225 the threshold N stress of vegetation above which symbiotic BNF occurs (unitless). $r_{BNF,s}$ for
226 crops is set greater than $r_{BNF,s}$ for natural PFTs and $b_{BNF,s} = 0$ for crops whereas $b_{BNF,s} > 0$ for
227 natural PFTs to account for the artificial selection of N-fixing crops over 4,000 years (O'Hara,

228 1998). $f(T) = \max\left(0, \left(\frac{44.83 - T}{44.83 - 32.72}\right)\left(\frac{T - 1.3}{32.72 - 1.3}\right)^{\frac{32.72 - 1.3}{44.83 - 32.72}}\right)$ is the temperature dependence

229 function from (Bytnerowicz et al., 2022) (unitless), where T is soil temperature of the top soil
230 layer (°C). B_s as a function of varying N_{stress} (assuming constant T) is illustrated in Figure S2a.

231   N stress of vegetation is determined by N demand of vegetation relative to root uptake of
232 soil NH_4^+ and NO_3^-:

233 $$N_{stress} = \max\left(0, \min\left(\frac{\Delta_V - U}{\Delta_V}, 1\right)\right) \tag{6}$$

234 N_{stress} varies between 0 and 1. When root uptake of soil NH_4^+ and NO_3^- (U) meets or exceeds N
235 demand of vegetation (Δ_V), then $N_{stress} = 0$ indicating no N stress. When root uptake of soil
236 NH_4^+ and NO_3^- is zero, then $N_{stress} = 1$ indicating maximum N stress. When $0 < U < \Delta_V$ then
237 $0 < N_{stress} < 1$. N_{stress} as a function of varying Δ_V (assuming constant U) is illustrated in
238 Figure S2b.

239   Finally, the C cost of symbiotic BNF is a component of autotrophic respiration and is
240 added to maintenance respiration from the root C pool:

241 $$C_{BNF} = B_s \kappa \left[\frac{1}{1000}\right] \tag{7}$$

242 C_{BNF} is the C cost of symbiotic BNF (kg C m^{-2} day^{-1}), κ is the per unit C cost of symbiotic BNF
243 (assumed to be 6.5 g C g N^{-1} (Minchin & Witty, 2005)), and $\left[\frac{1}{1000}\right]$ converts the units from g C to
244 kg C.

245   Note that, in the previous static representation of BNF in CLASSIC, BNF was not
246 separated into its free-living and symbiotic components – it was represented as a function of soil
247 temperature and soil moisture that contributed to the soil NH_4^+ pool (Asaadi & Arora, 2021).

248   2.3.2 Vegetation C:N ratio

249   The C:N ratios for each vegetation component and thus the C:N ratio of vegetation
250 evolve freely in response to changing C and N supply. N demand of a given vegetation
251 component depends on its prescribed minimum C:N ratio (Equations 1 and 3). When C supply is
252 high relative to N supply, vegetation component C:N ratios increase, whereas, when C supply is
253 low relative to N supply, vegetation component C:N ratios decrease. Additionally, prescribed
254 maximum vegetation component C:N ratios as well as the leaf N pool are used to calculate
255 photosynthetic capacity (Section 2.3.3).

256   The prescribed minimum and maximum leaf C:N ratios are based on Kerkhoff et al.,
257   2006; McGroddy et al., 2004, minimum and maximum stem C:N ratios are based on Weedon et
258   al., 2009, and minimum and maximum root C:N ratios are based on Yuan et al., 2011.

259   2.3.3 Photosynthetic capacity downregulation

260   Maximum rate of carboxylation is a function of leaf N:

261
$$V_{cmax} = \Lambda \left(\Gamma_1 \frac{N_L}{LAI} + \Gamma_2 \right) \tag{8}$$

262   V_{cmax} is the maximum rate of carboxylation (μmol CO_2 m^{-2} sec^{-1}), Λ describes the reduction in
263   V_{cmax} when current vegetation component C:N ratios exceed prescribed maximum C:N ratios
264   (unitless), Γ_1 is a PFT-dependent parameter from Kattge et al., 2009 (μmol CO_2 g N^{-1} sec^{-1}), LAI
265   is leaf area index (m^2 m^{-2}), and Γ_2 is a PFT-dependent parameter from Kattge et al., 2009 (μmol
266   CO_2 m^{-2} sec^{-1}). Note that, previously in Asaadi & Arora, 2021, Γ_1, Γ_2, and LAI were assumed to
267   be global constants. Here, Γ_1 and Γ_2 are PFT-dependent parameters and LAI is simulated
268   prognostically for each PFT.

269   The reduction in V_{cmax} when current vegetation component C:N ratios exceed prescribed
270   maximum C:N ratios is determined by the difference in current C:N ratio to prescribed maximum
271   C:N ratio for all vegetation components:

272
$$\Lambda = \exp \left(-k_\Lambda \left(\sum_i \frac{^1/_{C:N_{i,max}}}{\sum_i {}^1/_{C:N_{i,max}}} \max\left(0, C\!:\!N_i - C\!:\!N_{i,max}\right) \right) \right) \tag{9}$$

273   k_Λ is a parameter describing the strength of the reduction in V_{cmax} when $C\!:\!N_i$ exceeds $C\!:\!N_{i,max}$
274   (unitless), $C\!:\!N_i$ is the current C:N ratio of vegetation component i (kg C g N^{-1}), and $C\!:\!N_{i,max}$ is
275   the maximum C:N ratio of vegetation component i (kg C g N^{-1}). Λ varies between 0 and 1. When
276    $C\!:\!N_i$ do not exceed $C\!:\!N_{i,max}$ for all vegetation components, $\Lambda = 1$ indicating no reduction in
277   V_{cmax}. When $C\!:\!N_i$ exceeds $C\!:\!N_{i,max}$ for some or all vegetation components, $0 < \Lambda < 1$ and
278   V_{cmax} is reduced. This provides a feedback that reduces photosynthetic capacity further than
279   would be obtained from only the reduction in N_L in Equation 8 when the current vegetation C:N
280   ratio is high.

281   **3 Methodology**

282   3.1 CLASSIC simulations and forcing data sets

283   The simulations performed for this study used atmospheric CO_2 concentration,
284   meteorological, population density, land use change, N deposition, and N fertilisation forcings
285   based on the TRENDY protocol for 2019 and are described in Text S2. Annual TRENDY
286   simulations contribute to the Global Carbon Project (Friedlingstein et al., 2019). We first
287   performed a pre-industrial spin up using atmospheric CO_2 concentration, population density,
288   land cover, N deposition, and N fertilisation forcings corresponding to the year 1700. In the
289   absence of meteorological forcing before 1901, we used meteorological forcing from 1901 to
290   1925 repeatedly until the C and N pools came into equilibrium. Thresholds of 0.05 Pg C yr^{-1} for
291   the global net atmosphere-land CO_2 flux and 0.5 Tg N yr^{-1} for the global net atmosphere-land N
292   flux were used to assess if equilibrium was achieved.

293   We launched two sets of simulations with initial conditions from the pre-industrial spin
294 up. The first set of simulations consist of elevated CO_2 and N fertilisation experiments. For these
295 simulations, we followed the protocol outlined in Davies-Barnard et al., 2020, allowing the
296 comparison of our simulations to their results. First, we simulated the period from 1701 to 1995
297 (using meteorological forcing from 1901 to 1925 repeated eight times for the period from 1701
298 to 1900). Then, for the period from 1996 to 2015, we simulated an instantaneous 200 ppm
299 increase in CO_2 relative to normal historical CO_2 values. Similarly, we simulated an
300 instantaneous 50 kg N ha^{-1} yr^{-1} increase in N deposition relative to normal historical N deposition
301 values. Finally, we simulated the period from 1996 to 2015 with normal historical CO_2 and N
302 deposition values. All other forcings (meteorological, population density, land cover, and N
303 fertilisation) for the period from 1996 to 2015 follow their normal historical values. The effects
304 of elevated CO_2 and N fertilisation were calculated by differencing the results from the elevated
305 CO_2 and N fertilisation experiments over the period from 1996 to 2015 with the results from the
306 simulation with normal historical CO_2 and N deposition values over the period from 1996 to
307 2015.

308   The second set of simulations consist of historical simulations for the period from 1701 to
309 2018 in which we examined the effect of global change drivers concurrently and individually.
310 The global change drivers that we examined are atmospheric CO_2 concentration, N deposition,
311 climate, and land use change (which is characterized by changing crop area and N fertiliser
312 application) (Figure 1). Table S2 describes the forcings for each simulation. Note that, because
313 population density only affects fire and the overall effect of fire on C cycling is much smaller
314 than those of other global change drivers, we do not evaluate the population density forcing
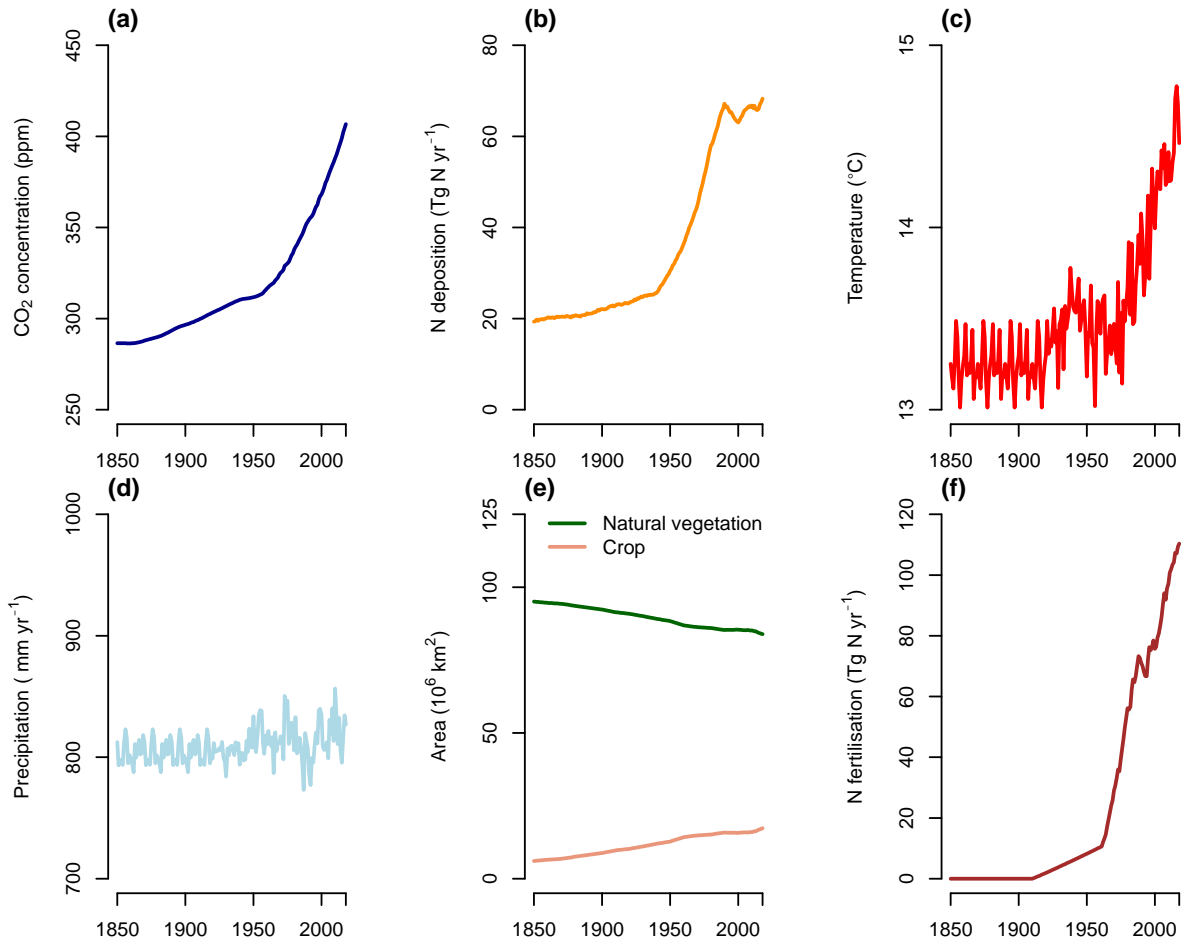315 individually and it follows its normal historical values in all simulations.

Figure 1. Globally-averaged values of the studied global change drivers over the period from 1701 to 2018. (a) Atmospheric CO_2 concentration. (b) N deposition. (c) Temperature. (d) Precipitation. (e) Global land area covered by natural vegetation and crops. (f) N fertiliser application.

321   We conducted all simulations with three versions of CLASSIC. The first version,
322   CLASSIC, is the standard land model with coupled C and N cycling. The second version,
323   CLASSIC-statN, is a modification of CLASSIC in which the regulation of BNF by N limitation
324   is turned off. While in CLASSIC symbiotic BNF is a function of time-evolving N_{stress} (Equation
325   5), in CLASSIC-statN symbiotic BNF is represented as a function of temperature and the
326   globally-averaged N_{stress} over the pre-industrial spin up (0.1):

327       $B_s = r_{BNF,s} f(T)(0.1)$ (10)

328   As a result, symbiotic BNF in CLASSIC-statN is unresponsive to changes in N_{stress} that are
329   associated with changing N limitation.

330   The third version, CLASSIC-C, has N cycling turned off and the downregulation of
331   photosynthetic capacity due to N limitation under elevated atmospheric CO_2 concentration is
332   controlled by an empirical parameter as explained in Arora et al., 2009; Asaadi & Arora, 2021.
333   Briefly, this empirical parameter, which ranges between 0 and 0.9, determines the rate of
334   increase of photosynthesis with increasing atmospheric CO_2 concentration. When it is set to 0,
335   photosynthesis does not increase with increasing atmospheric CO_2 concentration. When it is set
336   to 0.9, photosynthesis increases with increasing atmospheric CO_2 concentration at an
337   unconstrained rate that is determined by CLASSIC's photosynthesis equations which are based
338   on the standard biochemical model of photosynthesis in Collatz et al., 1991, 1992; Farquhar et
339   al., 1980. Here, we set this empirical parameter to 0.35 to yield a global net atmosphere-land
340   CO_2 flux that lies within the uncertainty range of estimates from the Global Carbon Project
341   (Friedlingstein et al., 2019). The uncertainty associated with this empirical parameter and this
342   representation of the downregulation of photosynthetic capacity due to N limitation under
343   elevated atmospheric CO_2 concentration motivated the implementation of coupled C and N
344   cycling in CLASSIC (Asaadi & Arora, 2021).

345   3.2 Evaluation

346   We compared simulated C and N pools and fluxes to observation-based estimates (Beer
347   et al., 2010; Davies-Barnard & Friedlingstein, 2020; Fowler et al., 2013; Friedlingstein et al.,
348   2019; Herridge et al., 2008; Köchy et al., 2015; Martens et al., 2017; Vitousek et al., 2013; Xu et
349   al., 2021). We compared the globally-averaged response of simulated NPP to elevated CO_2
350   (+200 ppm) and N fertilisation (+50 kg N ha^{-1} yr^{-1}) against estimates from (Song et al., 2019),
351   which is a meta-analysis of manipulative experiments that recorded how NPP responds to global
352   change drivers. We compared the globally-averaged response of simulated BNF to elevated CO_2
353   (+200 ppm) against estimates from (Liang et al., 2016), a meta-analysis of manipulative
354   experiments that recorded how BNF responds to elevated CO_2. We compared the globally-
355   averaged response of simulated BNF to N fertilisation (+50 kg N ha^{-1} yr^{-1}) against estimates from
356   (Zheng et al., 2019), a meta-analysis of manipulative experiments that recorded how BNF
357   responds to N fertilisation. We used results for natural ecosystems from the dataset in (Liang et
358   al., 2016), whereas (Song et al., 2019) and (Zheng et al., 2019) report results for natural
359   ecosystems exclusively. We also compared the response of NPP and BNF to elevated CO_2 and N
360   fertilisation in CLASSIC simulations to results from five CMIP6 (Coupled Model
361   Intercomparison Project Phase 6; Eyring et al., 2016) land models described in (Davies-Barnard
362   et al., 2020) – the Community Land Model version 4.5 (CLM4.5), the Community Land Model
363   version 5 (CLM5), the JSBACH version 3.20 model, the Joint UK Land Environment Simulator
364   version 5.4 (JULES-ES), and the Lund-Potsdam-Jena General Ecosystem Simulator version 4.0

365 (LPJ-GUESS). These land models represent coupled C and N cycling and implement different
366 representations of key N cycling processes, including their representation of BNF (Table S3).
367 Note that, among these land models, CLM5 is the only land model that distinguishes between
368 free-living and symbiotic BNF and that captures the regulation of BNF by N limitation.

369 **4 Results and discussion**

370   4.1 BNF evaluation

371   CLASSIC reproduces global pre-industrial total BNF (free-living and symbiotic),
372 present-day free-living BNF, present-day natural symbiotic BNF, and present-day crop BNF
373 reasonably well in comparison to observation-based estimates and other CMIP6 land models
374 (Figure 2). CLASSIC simulates 64 Tg N yr^{-1} for pre-industrial total BNF, which is comparable to
375 estimates of 58 Tg N yr^{-1} (40 – 100 Tg N yr^{-1}) from (Vitousek et al., 2013). Simulated present-
376 day free-living BNF (23 Tg N yr^{-1}) and present-day natural symbiotic BNF (47 Tg N yr^{-1}) are
377 also comparable to estimates of 31 Tg N yr^{-1} (21 – 66 Tg N yr^{-1}) and 57 Tg N yr^{-1} (31 – 66 Tg N
378 yr^{-1}), respectively, from (Davies-Barnard & Friedlingstein, 2020). As such, CLASSIC simulates
379 70 Tg N yr^{-1} for present-day natural BNF (combined free-living and natural symbiotic). This is
380 similar to estimates from CLM4.5, CLM5, JSBACH, JULES-ES, and LPJ-GUESS, which range
381 from 46 to 107 Tg N yr^{-1} (Table S4), as well as to other CMIP6 land models, such as 73 – 122 Tg
382 N yr^{-1} by CABLE (Peng et al., 2020) and 37 – 117 Tg N yr^{-1} by O-CN (Meyerholt et al., 2020).
383 Simulated present-day crop symbiotic BNF (74 Tg N yr^{-1}) is comparable to estimates of 50 – 70
384 Tg N yr^{-1} from (Herridge et al., 2008).

385   Free-living BNF is greatest in tropical biomes (Figure 2d) due to higher temperatures.
386 Natural symbiotic BNF is greatest in tropical biomes (Figure 2e), as expected (Hedin et al.,
387 2009). Natural symbiotic BNF is higher in tropical America than in tropical Africa and Asia,
388 corresponding to higher N deposition in tropical Africa and Asia (Figure S3) which relieves N
389 limitation. Crop symbiotic BNF is greatest in regions with high crop area (Figure 2f, Figure S4).
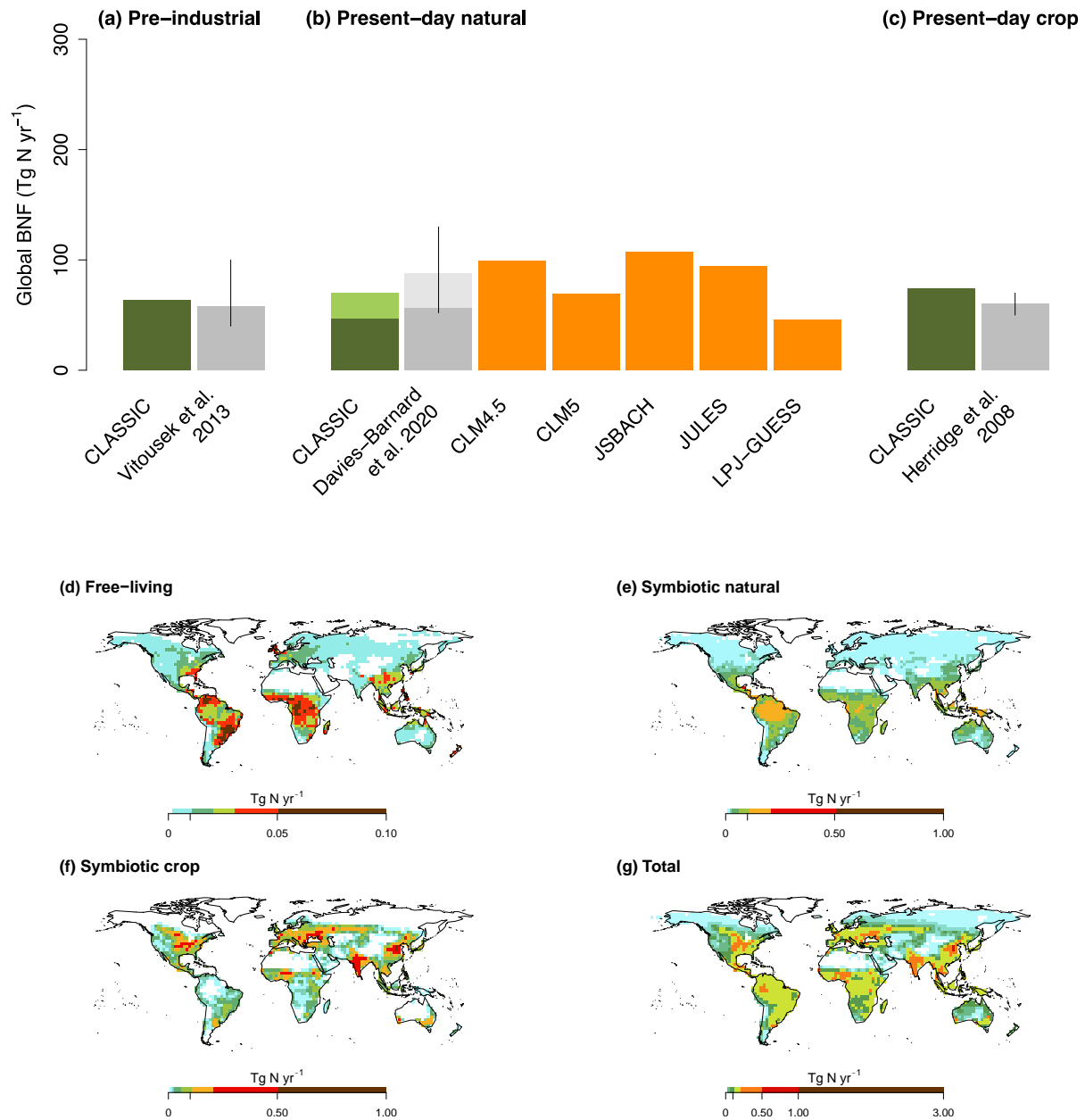
Figure 2. Biological nitrogen fixation simulated by CLASSIC, observation-based estimates from Davies-Barnard & Friedlingstein, 2020; Herridge et al., 2008; Vitousek et al., 2013, and estimates from other CMIP6 land models (CLM4.5, CLM5, JSBACH, JULES-ES, and LPJ-GUESS; Davies-Barnard et al., 2020). (a) Global pre-industrial biological nitrogen fixation (averaged over 1701 to 1721). (b) Global present-day natural biological nitrogen fixation (averaged over 1998 to 2018). When free-living and natural symbiotic biological nitrogen fixation are differentiated, they are distinguished by lighter and darker colours respectively. (c) Global present-day crop symbiotic biological nitrogen fixation (averaged over 1998 to 2018). Geographical distribution of present-day (d) free-living biological nitrogen fixation, (e) natural symbiotic biological nitrogen fixation, and (f) crop symbiotic biological nitrogen fixation (averaged over 1998 to 2018).

403   Few land models incorporate an explicit representation of free-living BNF, combining it
404 with natural symbiotic BNF. However, observations suggest that free-living BNF may be a
405 substantial N input to terrestrial ecosystems. Reed et al., 2011 suggests that free-living BNF rates
406 are comparable to natural symbiotic BNF rates in some terrestrial ecosystems. Elbert et al., 2012
407 suggests that cryptogamic covers (N-fixing photoautotrophic communities that cover terrestrial
408 surfaces) account for 49 Tg N yr^{-1}, while Davies-Barnard & Friedlingstein, 2020 suggests that
409 global free-living BNF is 31 Tg N yr^{-1} (21 – 66 Tg N yr^{-1}) and contributes ~35% of natural BNF.
410 Because free-living BNF is not directly influenced by N limitation, its distinction from natural
411 symbiotic BNF is important for representing the dynamic response of vegetation to N limitation.

412   4.2 Elevated CO_2 and N fertilisation experiments

413   4.2.1 NPP response to elevated CO_2 and N fertilisation

414   The NPP response to elevated CO_2 (+200 ppm) simulated by CLASSIC was +11.3%,
415 which is consistent with observation-based estimates (+15.6%; Song et al., 2019) (Figure 3a).
416 This estimate also lies in the range of other CMIP6 land models (+5 to +20%; Davies-Barnard et
417 al., 2020). The NPP response to N fertilisation (+50 kg N ha^{-1} yr^{-1}) simulated by CLASSIC was
418 +16.1%, which is higher than observation-based estimates (+6.5%; Song et al., 2019) (Figure
419 3c). Other CMIP6 land models overestimated (CLM4.5, CLM5, and LPJ-GUESS) or
420 underestimated (JSBACH and JULES) the NPP response to N fertilisation (Davies-Barnard et
421 al., 2020).

422   CLASSIC-statN had a lower NPP response to elevated CO_2 (+7.5%) than that of
423 CLASSIC because BNF is not upregulated in response to stronger N limitation due to elevated
424 CO_2 in CLASSIC-statN. Similarly, CLASSIC-statN had a higher NPP response to N fertilisation
425 (+20.8%) than that of CLASSIC because BNF is not downregulated in response to weaker N
426 limitation due to N fertilisation in CLASSIC-statN. CLASSIC-C had a higher NPP response to
427 elevated CO_2 (+22.7%) than that of CLASSIC. CLASSIC-C had no response to N fertilisation
428 because there is no N limitation.
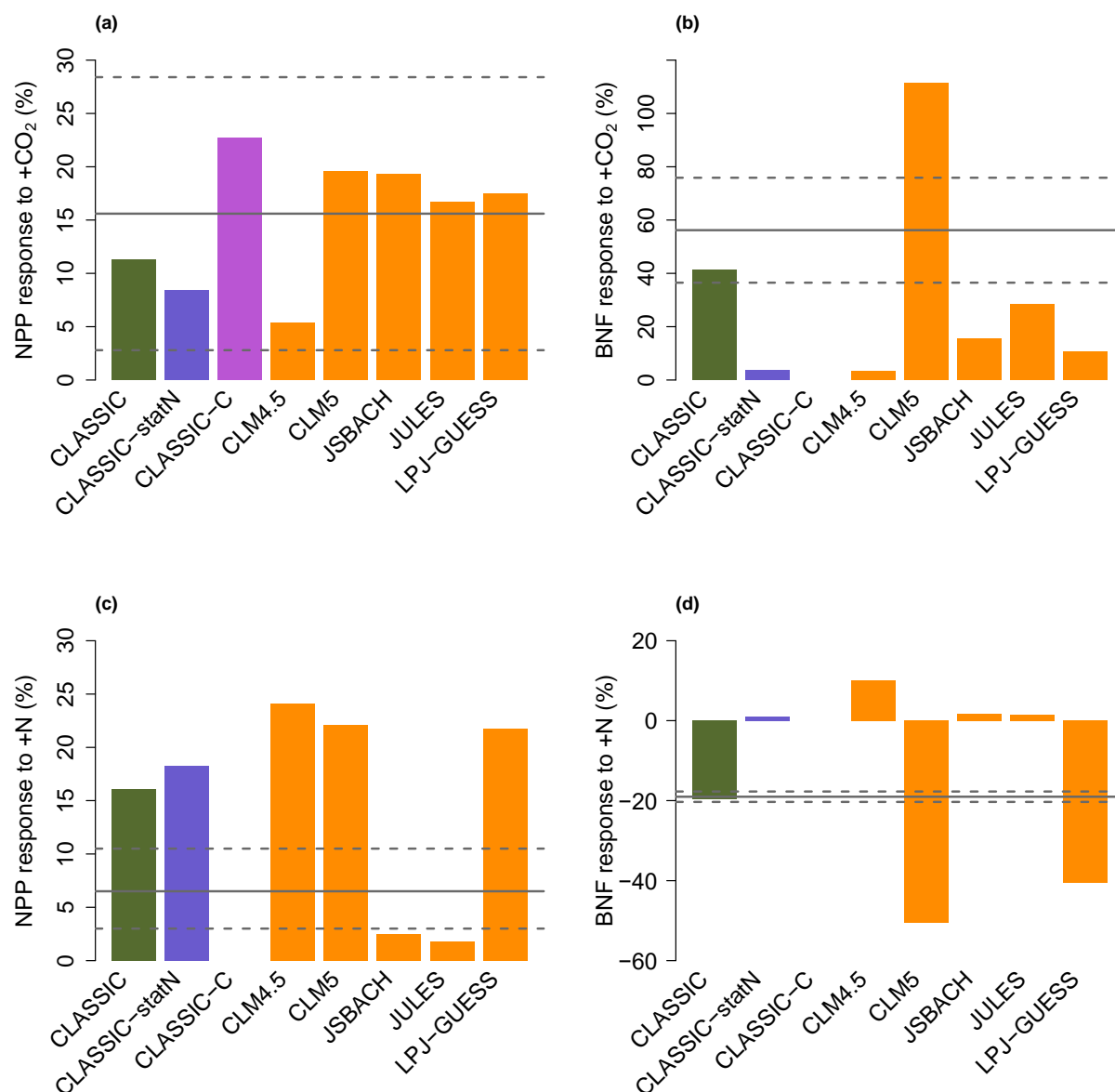
429

Figure 3. Response of (a) net primary productivity to elevated CO_2 (+200 ppm), (b) biological nitrogen fixation to elevated CO_2 (+200 ppm), (c) net primary productivity to nitrogen fertilisation (+50 kg N ha^{-1} yr^{-1}), and (d) biological nitrogen fixation to nitrogen fertilisation (+50 kg N ha^{-1} yr^{-1}) simulated by CLASSIC, CLASSIC without the regulation of BNF by N limitation (CLASSIC-statN), and CLASSIC without N cycling (CLASSIC-C). These estimates are compared to estimates from other CMIP6 land models (CLM4.5, CLM5, JSBACH, JULES, and LPJ-GUESS) and observation-based estimates from meta-analyses (indicated by the gray horizontal lines where the solid line indicates the mean and the dashed lines indicate the 95% confidence intervals). Observation-based estimates for the response of net primary productivity are from (Song et al., 2019), observation-based estimates for the response of biological nitrogen fixation to elevated CO_2 are from (Liang et al., 2016), and observation-based estimates for the

441   response of biological nitrogen fixation to nitrogen fertilisation (+50 kg N ha^{-1} yr^{-1}) are from

442   (Zheng et al., 2019). Results are averaged over 1996 to 2015.

443   The response of NPP to elevated CO_2 decreases with increasing absolute latitude.
444 Individual grid cells exhibit a lower NPP response to elevated CO_2 with increasing absolute
445 latitude (Figure 4a; $P < 0.001$). This is due to the temperature dependence of photosynthesis
446 which implies that the response of NPP to elevated CO_2 is stronger at higher temperatures
447 consistent with observations (Baig et al., 2015; Long, 1991). Additionally, because the growing
448 season is longer at lower latitudes than at higher latitudes, the response of NPP to elevated CO_2
449 is realised over a longer period at lower latitudes than at higher latitudes.

450   In contrast, the response of NPP to N fertilisation increases with increasing absolute
451 latitude. Individual grid cells exhibit a higher NPP response to N fertilisation with increasing
452 absolute latitude (Figure 4b; $P < 0.001$). Examining the response of NPP to N fertilisation allows
453 for the assessment of N limitation (Sullivan et al., 2014). Higher latitude vegetation is suggested
454 to be more N-limited than lower latitude vegetation (Brookshire et al., 2012; Du et al., 2020;
455 LeBauer & Treseder, 2008). CLASSIC simulates a significantly stronger response to N
456 fertilisation at high latitudes than at low latitudes, suggesting stronger N limitation at high
457 latitudes than at low latitudes (Figure 4b). Thus, the stronger response to elevated CO_2 at low
458 latitudes than at high latitudes is not only driven by the temperature dependence of
459 photosynthesis (as described above) but also occurs because low latitudes are less N-limited than
460 high latitudes. This causes the bimodality of the response of NPP at the grid cell scale, i.e., that
461 NPP of a given grid cell tends to respond to either elevated CO_2 or to N fertilisation but not to
462 both elevated CO_2 and N fertilisation (Figure 4c). This behaviour is consistent with that of other
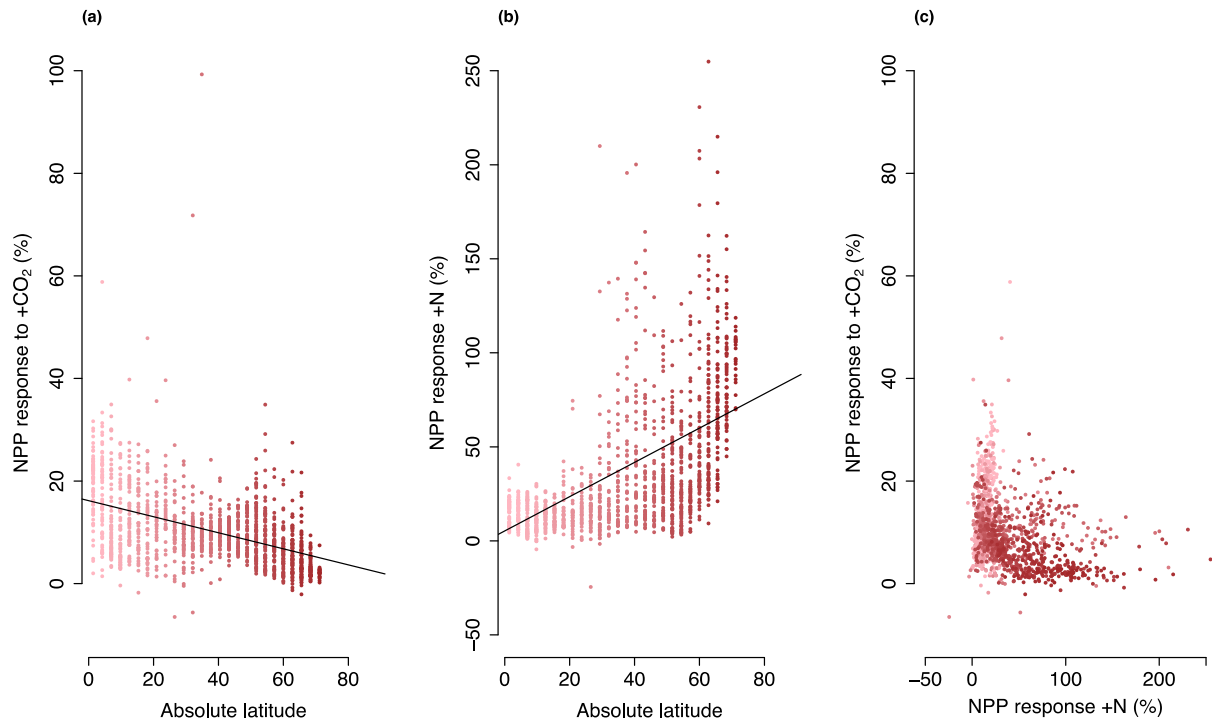463 CMIP6 land models (Davies-Barnard et al., 2020).

464
465 **Figure 4.** Responses of net primary productivity to elevated CO_2 (+200 ppm) and nitrogen
466 fertilisation (+50 kg N ha^{-1} yr^{-1}) at the grid cell scale. (a) Response of net primary productivity to
467 elevated CO_2 simulated by CLASSIC as a function of absolute latitude. (b) Response of net
468 primary productivity to nitrogen fertilisation simulated by CLASSIC as a function of absolute
469 latitude. (c) Net primary productivity response to both elevated CO_2 and nitrogen fertilisation
470 simulated by CLASSIC. Each point represents an individual grid cell. Lighter colours represent
471 lower latitudes and darker colours represent higher latitudes. Results are averaged over 1996 to
472 2015.

473   4.2.2 BNF response to elevated CO_2 and N fertilisation

474   The BNF response to elevated CO_2 (+200 ppm) simulated by CLASSIC was +41.4%,
475 which is consistent with observation-based estimates (+56.2%; Liang et al., 2016) (Figure 3b).
476 This is a more accurate response than other CMIP6 land models, which all lie outside this range:
477 CLM5 overestimated the BNF response to elevated CO_2 and CLM4.5, JSBACH, JULES-ES and
478 LPJ-GUESS underestimated the BNF response to elevated CO_2 (Davies-Barnard et al., 2020).
479 The BNF response to N fertilisation (+50 kg N ha^{-1} yr^{-1}) simulated by CLASSIC was –19.7%,
480 which is consistent with observation-based estimates (–19%; Zheng et al., 2019) (Figure 3d).
481 Other CMIP6 land models either overestimated (CLM5, and LPJ-GUESS) or underestimated
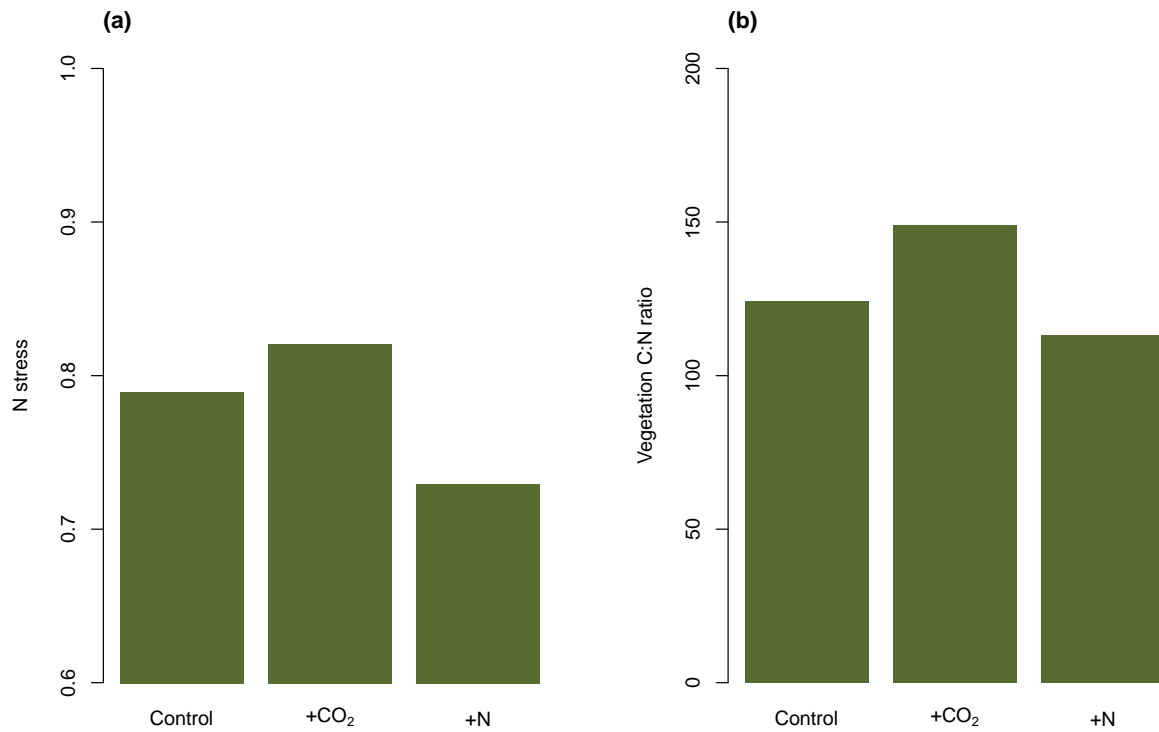482 (CLM4.5, JSBACH, and JULES) the BNF response to N fertilisation (Davies-Barnard et al.,
483 2020).

484   The BNF response in CLASSIC is regulated by N limitation (represented as N stress in
485 Equations 5 and 6), which increases under elevated CO_2 and decreases under N fertilisation in
486 comparison to estimates from under normal historical CO_2 and N deposition values (Figure 5a).
487 This follows observations that elevated CO_2 intensifies N limitation (Luo et al., 2004), whereas
488 N fertilisation relieves N limitation (LeBauer & Treseder, 2008).

489   4.2.3 Overall response to elevated CO_2 and N fertilisation

490   In comparison to other CMIP6 land models (Davies-Barnard et al., 2020), CLM5 is the
491 sole other land model represented BNF regulation by N limitation (Table S3); CLM4.5,
492 JSBACH, JULES-ES and LPJ-GUESS represent BNF with empirical relationships between BNF
493 and NPP (CLM4.5, JSBACH, and JULES-ES) or BNF and ET (LPJ-GUESS). Similar to
494 CLASSIC, CLM5 estimated the expected directions of the BNF response to elevated CO_2 and N
495 fertilisation (i.e., increase and decrease) but overestimated BNF change under both elevated CO_2
496 and N fertilisation, whereas CLASSIC underestimated BNF change under N fertilisation (Figure
497 3).

498   In addition to regulating symbiotic BNF, plants can respond dynamically to N limitation
499 by increasing vegetation component C:N ratios (Elser et al., 2010; Sistla & Schimel, 2012).
500 Elevated CO_2 can increase the vegetation C:N ratio due to stimulated photosynthesis. N
501 fertilisation can decrease the vegetation C:N ratio due to "luxury" uptake of N. As such,
502 representing a flexible vegetation C:N ratio in land models results in the greatest agreement with
503 observations (Meyerholt & Zaehle, 2015). In CLASSIC, vegetation C:N ratio increases under
504 elevated CO_2 and decreases under N fertilisation in comparison to estimates from under normal
505 historical CO_2 and N deposition values (Figure 5b).

506   Having established confidence in CLASSIC's response to elevated CO_2 and N
507 fertilisation experiments we now evaluate CLASSIC's response to global change drivers over the
508 historical period.

(a)   **(b)**

509

Figure 5. (a) Nitrogen stress and (b) vegetation carbon to nitrogen ratio under elevated CO_2
(+200 ppm) and under nitrogen fertilisation (+50 kg N ha^{-1} yr^{-1}) simulated by CLASSIC. These
estimates are compared to estimates under normal historical CO_2 and nitrogen deposition values
(control) simulated by CLASSIC. Results are averaged over 1996 to 2015.

514   4.3 Historical simulations

515   4.3.1 Individual global change drivers over the historical period

516   Similar to their responses in the elevated CO_2 experiment (+200 ppm CO_2), NPP and
517   natural symbiotic BNF increase in the simulation driven with atmospheric CO_2 concentration
518   acting in isolation over the historical period (Figure 6ab). NPP increases because elevated
519   atmospheric CO_2 concentration stimulates photosynthesis (Collatz et al., 1991, 1992; Farquhar et
520   al., 1980), i.e., CO_2 fertilisation (Walker et al., 2020). The increase in natural symbiotic BNF is
521   due to an increase in N stress (Figure 6d). This follows observations that increased atmospheric
522   CO_2 concentration intensifies N limitation (Luo et al., 2004; Terrer et al., 2019). Vegetation C:N
523   ratio also increases due to increased C supply (Figure 6e) consistent with observations (Elser et
524   al., 2010; Sistla & Schimel, 2012). Including N cycling reduces the NPP change when
525   atmospheric CO_2 concentration is acting in isolation over the historical period: the NPP change
526   for CLASSIC (5.6 Pg C yr^{-1}) is 45% that of CLASSIC-C (12.4 Pg C yr^{-1}). Furthermore, when
527   BNF is not regulated by N limitation, the NPP change when atmospheric CO_2 concentration is
528   acting in isolation over the historical period is even lower: the NPP change for CLASSIC-statN
529   (3.5 Pg C yr^{-1}) is 28% that of CLASSIC-C (12.4 Pg C yr^{-1}).

530   Similar to their responses in the N fertilisation experiment (+50 kg N ha^{-1} yr^{-1}), NPP
531   increases slightly and natural symbiotic BNF decreases slightly in the simulation driven with N
532   deposition acting in isolation over the historical period (Figure 6ab). NPP increases because
533   elevated N deposition stimulates photosynthesis by increasing leaf N (Equations 8 and 9). The
534   decrease in natural symbiotic BNF is due to a decrease in N stress (Figure 6d). This follows
535   observations that increased N deposition relieves N limitation (LeBauer & Treseder, 2008). The
536   changes in NPP and natural symbiotic BNF are low in comparison to those from the N
537   fertilisation experiment because the globally-averaged change in N deposition over the historical
538   period (+1.6 kg N ha^{-1} yr^{-1} between pre-industrial and present-day values) is much lower than the
539   N fertilisation treatment (+50 kg N ha^{-1} yr^{-1}).

540   Both NPP and natural symbiotic BNF increase slightly in the simulation driven with
541   climate acting in isolation over the historical period (Figure 6ab). NPP increases, first, because
542   elevated temperature stimulates photosynthesis and increases the length of the growing season
543   and, second, because elevated precipitation relieves water limitation (although change in
544   precipitation over the historical period is geographically variable with some regions experiencing
545   increased precipitation and other regions experiencing decreased precipitation (Lau et al., 2013)).
546   Additionally, elevated temperature and precipitation stimulate N mineralisation (Figure S5)
547   which stimulates photosynthesis by increasing leaf N (Equations 8 and 9). The increase in
548   natural symbiotic BNF occurs despite a slight decrease in N stress (Figure 6d). This slight
549   decrease in N stress is likely due to elevated N mineralisation which overcomes the influence of
550   elevated temperature and precipitation on stimulating photosynthesis, increasing the length of the
551   growing season, and relieving water limitation which would all cause an increase in N stress.
552   Given these counteracting drivers, the change in N stress is minimal. The increase in natural
553   symbiotic BNF is thus due to elevated temperature because symbiotic BNF is a function of
554   temperature as well as N stress (Equation 6).

555   In the simulation driven with land use change acting in isolation over the historical period
556   (which includes both changing crop area and N fertiliser application), NPP increases and crop
557   symbiotic BNF increases but natural symbiotic BNF decreases (Figure 6ac). This is due to higher

558   photosynthetic capacity of crops than of natural vegetation (Table S1; Kattge et al., 2009),

559   increasing crop area, and decreasing natural vegetation area, respectively. Note that the increase

560   in crop symbiotic BNF occurs because increasing crop area more than compensates for

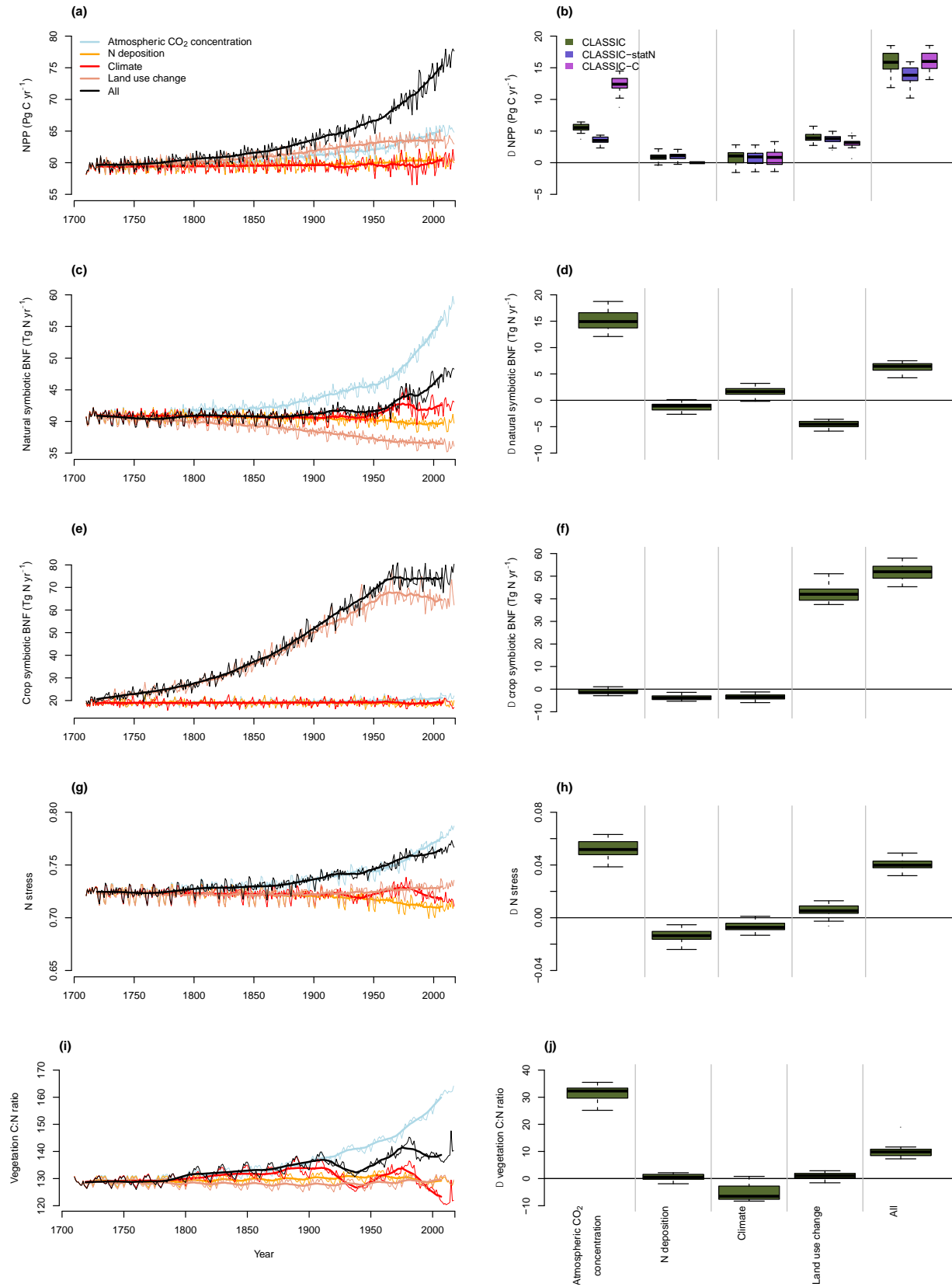561   increasing N fertiliser application which decreases N stress of crops.

562

563 **Figure 6.** Net primary productivity, symbiotic biological nitrogen fixation, nitrogen stress, and
564 vegetation carbon to nitrogen ratio over the historical period simulated by CLASSIC, CLASSIC
565 without the regulation of BNF by N limitation (CLASSIC-statN), and CLASSIC without N
566 cycling (CLASSIC-C) for all global change drivers concurrently and individually. (a), (c), (e)
567 and (g). Time series simulated by CLASSIC. (b), (d), (f), and (h). Change from pre-industrial
568 (averaged over 1701 to 1721) to present-day (1998 to 2018) estimates simulated by CLASSIC,
569 CLASSIC-statN, and CLASSIC-C (where the solid line indicates the median and the box extends
570 from the first quartile to the third quartile).

571   4.3.2 All global change driver concurrently over the historical period

572   CLASSIC reproduces observation-based estimates for global C and N pools and fluxes in
573 the historical simulation when all global change drivers are acting concurrently, similarly to
574 CLASSIC-C. CLASSIC reproduces the latitudinal patterns of GPP, vegetation C, soil organic C,
575 and evapotranspiration (Figure 7). CLASSIC reproduces observation-based estimates of global N
576 inputs, i.e., BNF, (as described in Section 4.1) as well as observation-based estimates of global N
577 losses (Table S4, Figure S6). Furthermore, CLASSIC estimates agree with other CMIP6 land
578 models (Table S4).

579   The global net atmosphere-land CO_2 flux or net biome productivity (NBP) is the critical
580 determinant of the performance of a land model because it ultimately affects atmospheric CO_2
581 concentration. Estimates of NBP from CLASSIC, CLASSIC-statN, and CLASSIC-C all lie
582 within the uncertainty range of estimates from the Global Carbon Project (Friedlingstein et al.,
583 2019) and thus all three versions of CLASSIC successfully reproduce the terrestrial C sink over
584 the late 20th century and early 21st century (Figure 8a). NBP estimates for the present day (1998
585 to 2018) when all global change drivers are acting concurrently are similar for all three versions
586 of CLASSIC. The difference between these three versions of CLASSIC is in how each responds
587 to individual global change drivers and, in particular, to atmospheric CO_2 concentration (Figure
588 8c). Present-day NBP for CLASSIC-C when atmospheric CO_2 concentration is acting in
589 isolation is the highest (3.9 Pg C yr^{-1}). Including N cycling reduces NBP: present-day NBP for
590 CLASSIC (1.4 Pg C yr^{-1}) is 44% lower than CLASSIC-C (i.e., a decrease of 2.5 Pg C yr^{-1}).
591 Furthermore, when BNF is not regulated by N limitation, NBP is even lower: present-day NBP
592 for CLASSIC-statN (0.9 Pg C yr^{-1}) is 64% lower than CLASSIC-C (i.e., a decrease of 3.0 Pg C
593 yr^{-1}). When all global change drivers are acting concurrently, the difference in present-day NBP
594 between CLASSIC and CLASSIC-statN is 0.2 Pg C yr^{-1} (1.3 Pg C yr^{-1} vs. 1.1 Pg C yr^{-1}) and is
595 the direct result of upregulated BNF driven by stronger N limitation under elevated atmospheric
596 CO_2 concentration which alleviates N limitation to some extent.

597   Historical NBP estimates of CLASSIC-C, which is the original version of CLASSIC, lie
598 within the uncertainty range of estimates from the Global Carbon Project (Friedlingstein et al.,
599 2019) because the strength of its CO_2 fertilisation effect has been adjusted to do so. Present-day
600 NBP when atmospheric CO_2 concentration is acting in isolation is higher for CLASSIC-C than
601 for CLASSIC and CLASSIC-statN (Figure 8c). This is because CLASSIC-C has been adjusted
602 to compensate for the effects of N deposition and elevated N mineralisation (due to elevated
603 temperature) over the historical period on NBP. Both these processes should stimulate NPP by
604 alleviating N limitation to some extent but they are not explicitly represented in CLASSIC-C.
605 While the absence of interactions between C and N cycling can be "accounted for" in historical
606 simulations by adjusting the strength of the CO_2 fertilisation effect, it has critical consequences
607 for future simulations which will encompass interacting and amplifying global change drivers.
608 This emphasises the importance of explicitly representing N cycling and the dynamic response of
609 vegetation to N limitation in land models.
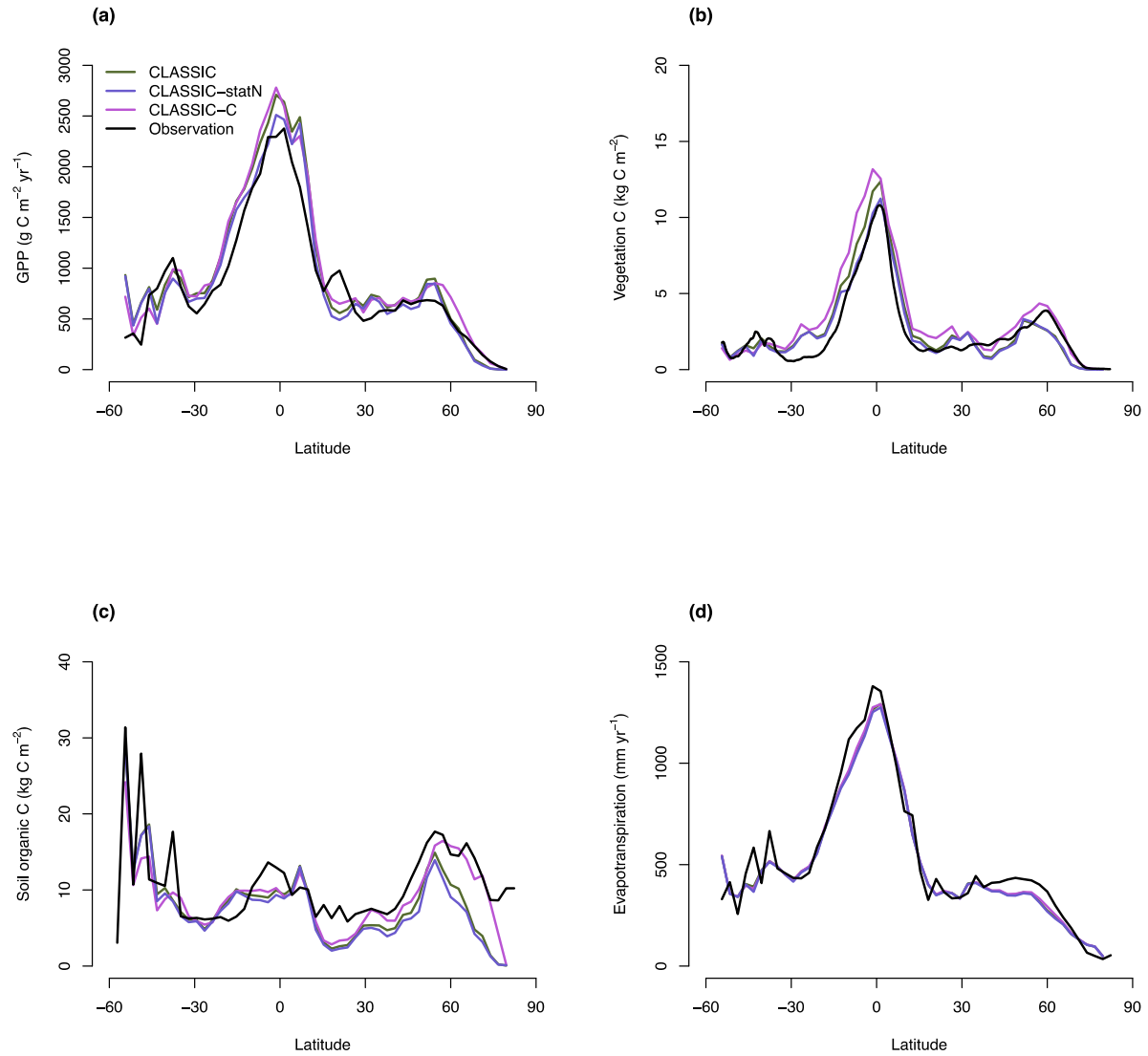
Figure 7. Latitudinal distributions of (a) gross primary productivity, (b) vegetation carbon, (c) soil organic carbon, and (d) evapotranspiration (averaged over 1998 to 2018) simulated by CLASSIC, CLASSIC without the regulation of BNF by N limitation (CLASSIC-statN), and CLASSIC without N cycling (CLASSIC-C). Observation-based estimates are from (Beer et al., 2010) for gross primary productivity, (Xu et al., 2021) for vegetation carbon, (Köchy et al., 2015) for soil organic carbon, and (Martens et al., 2017) for evapotranspiration. Time series are shown in Figure S7.
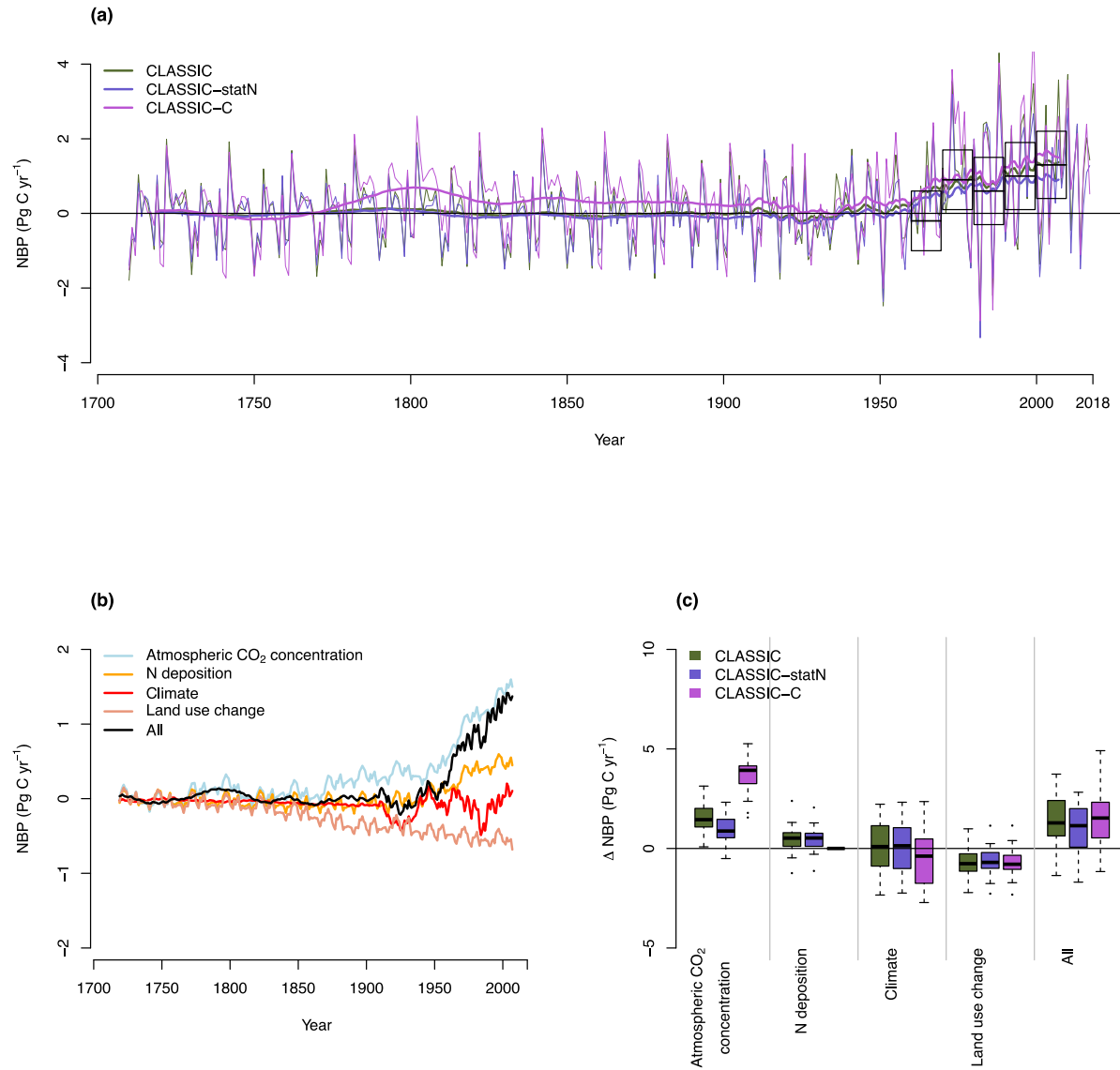
(a)

(b)

(c)

618
619 **Figure 8.** Net biome productivity over the historical period simulated by CLASSIC, CLASSIC
620 without the regulation of BNF by N limitation (CLASSIC-statN), and CLASSIC without N
621 cycling (CLASSIC-C). (a) Time series of net biome productivity simulated by CLASSIC,
622 CLASSIC-statN, and CLASSIC-C over the historical period from 1701 to 2018 for all global
623 change drivers concurrently. Boxes show the decadal mean and one standard deviation of
624 observation-based estimates from the Global Carbon Project (Friedlingstein et al., 2019). (b)
625 Time series of net biome productivity simulated by CLASSIC over the historical period from
626 1701 to 2018 for all global change drivers concurrently and individually. (c) Present-day (1998
627 to 2018) net biome productivity estimates simulated by CLASSIC, CLASSIC-statN, and
628 CLASSIC-C (where the solid line indicates the median and the box extends from the first
629 quartile to the third quartile).

5 Conclusions

Representing coupled C and N cycling in land models is a key challenge for projecting the terrestrial C sink. Although BNF is central to representing N cycling in land models given its key role in the dynamic response of vegetation to N limitation (Meyerholt et al., 2020; Peng et al., 2020; Wieder et al., 2015), it is challenging to evaluate simulated BNF against observation-based constraints due to the paucity of available data (Davies-Barnard & Friedlingstein, 2020). Simulating experimental manipulations of global change drivers and subsequently analysing the direction and magnitude of the response of BNF are an effective method for testing whether underlying mechanisms and thus the dynamic response of vegetation to N limitation via BNF are realistically represented. Our study shows that, without the regulation of BNF by N limitation, CLASSIC underestimates BNF increase under elevated CO_2 and simulates a BNF increase rather than a BNF decrease under N fertilisation. This leads to an underestimation of the NPP increase under elevated CO_2 and an overestimation of the NPP increase under N fertilisation, respectively. Without N cycling, CLASSIC overestimates NPP increase under elevated CO_2 and simulates no NPP change under N fertilisation.

Importantly, our study suggests that explicitly representing N cycling and the dynamic response of vegetation to N limitation of plant growth in land models is pivotal for realistically simulating the terrestrial C sink under global change. When the dynamic response of vegetation to N limitation via BNF is represented in CLASSIC, the present-day global net atmosphere-land CO_2 flux is decreased by 0.2 Pg C yr^{-1} in comparison to CLASSIC without N cycling. However, when the regulation of BNF by N limitation is not represented, the present-day global net atmosphere-land CO_2 flux is decreased by 0.4 Pg C yr^{-1} in comparison to CLASSIC without N cycling. The upregulation of BNF driven by stronger N limitation under elevated atmospheric CO_2 concentration thus alleviates N limitation. As such, representing the dynamic response of vegetation to N limitation via BNF increases the present-day terrestrial C sink by 0.2 Pg C yr^{-1}. Furthermore, while CLASSIC reproduces observations of the terrestrial C sink over the late 20th century and early 21st century regardless of whether N cycling is represented, CLASSIC without N cycling is only successful at doing so because the strength of the CO_2 fertilisation effect has been adjusted and thus compensates for the stimulatory influences of elevated N deposition and elevated N mineralisation (due to elevated temperature) on terrestrial C sequestration which are not represented. This has critical implications for projecting the future terrestrial C sink under interacting and amplifying global change drivers. Indeed, a former version of CLASSIC without N cycling (the coupled CLASS-CTEM framework) implemented within the 5th generation Canadian Earth System Model (CanESM5) yields one of the highest global net atmosphere-land CO_2 flux among CMIP6 Earth System Models under a high atmospheric CO_2 concentration scenario for the 21st century (Arora et al., 2020; Koven et al., 2021; Liddicoat et al., 2021). Thus, a mechanistic representation of N cycling and the dynamic response of vegetation to N limitation of plant growth in land models enables a more realistic representation of the response of the terrestrial C sink to global change drivers, providing confidence in projections of the future terrestrial C sink.

Acknowledgments

Open Research

The CLASSIC software container and all code for CLASSIC v.1.0 are available on the CLASSIC community Zenodo page (https://zenodo.org/communities/classic/?page=1&size=20).

References

Arora, V. K., & Boer, G. J. (2005a). A parameterization of leaf phenology for the terrestrial ecosystem component of climate models. *Global Change Biology*, *11*(1), 39–59. https://doi.org/10.1111/j.1365-2486.2004.00890.x

Arora, V. K., & Boer, G. J. (2005b). Fire as an interactive component of dynamic vegetation models. *Journal of Geophysical Research: Biogeosciences*, *110*(G2). https://doi.org/10.1029/2005jg000042

Arora, V. K., & Boer, G. J. (2010). Uncertainties in the 20th century carbon budget associated with land use change. *Global Change Biology*, *16*(12), 3327–3348. https://doi.org/10.1111/j.1365-2486.2010.02202.x

Arora, V. K., & Melton, J. R. (2018). Reduction in global area burned and wildfire emissions since 1930s enhances carbon uptake by land. *Nature Communications*, *9*(1), 1–10. https://doi.org/10.1038/s41467-018-03838-0

Arora, V. K., Boer, G. J., Christian, J. R., Curry, C. L., Denman, K. L., Zahariev, K., et al. (2009). The effect of terrestrial photosynthesis down regulation on the twentieth-century carbon budget simulated with the CCCma Earth System Model. *Journal of Climate*, *22*(22), 6066–6088. https://doi.org/10.1175/2009JCLI3037.1

Arora, V. K., Katavouta, A., Williams, R. G., Jones, C. D., Brovkin, V., Friedlingstein, P., et al. (2020). Carbon–concentration and carbon–climate feedbacks in CMIP6 models and their comparison to CMIP5 models. *Biogeosciences*, *17*(16), 4173–4222. https://doi.org/10.5194/bg-17-4173-2020

Asaadi, A., & Arora, V. K. (2021). Implementation of nitrogen cycle in the CLASSIC land model. *Biogeosciences*, *18*(2), 669–706. https://doi.org/10.5194/bg-18-669-2021

Asaadi, A., Arora, V. K., Melton, J. R., & Bartlett, P. (2018). An improved parameterization of leaf area index (LAI) seasonality in the Canadian Land Surface Scheme (CLASS) and Canadian Terrestrial Ecosystem Model (CTEM) modelling framework. *Biogeosciences*, *15*(22), 6885–6907. https://doi.org/10.5194/bg-15-6885-2018

Baig, S., Medlyn, B. E., Mercado, L. M., & Zaehle, S. (2015). Does the growth response of woody plants to elevated CO2 increase with temperature? A model-oriented meta-analysis. *Global Change Biology*, *21*(12), 4303–4319. https://doi.org/10.1111/gcb.12962

Beer, C., Reichstein, M., Tomelleri, E., Ciais, P., Jung, M., Carvalhais, N., et al. (2010). Terrestrial gross carbon dioxide uptake: Global distribution and covariation with climate. *Science*, *329*(5993), 834–838. https://doi.org/10.1126/science.1184984

710 Brookshire, E. N. J., Gerber, S., Menge, D. N. L., & Hedin, L. O. (2012). Large losses of
711   inorganic nitrogen from tropical rainforests suggest a lack of nitrogen limitation. *Ecology*
712   *Letters*, *15*(1), 9–16. https://doi.org/10.1111/j.1461-0248.2011.01701.x

713 Bytnerowicz, T. A., Akana, P., Griffin, K., & Menge, D. N. L. (2022). The temperature
714   sensitivity of woody dinitorgen fixation across species and growing temperatures. *Nature*
715   *Plants*. https://doi.org/10.1038/s41477-021-01090-x

716 Cheng, W., Parton, W. J., Gonzalez-Meler, M. A., Phillips, R., Asao, S., Mcnickle, G. G., et al.
717   (2014). Synthesis and modeling perspectives of rhizosphere priming. *New Phytologist*,
718   *201*(1), 31–44. https://doi.org/10.1111/nph.12440

719 Collatz, G. J., Ball, J. T., Grivet, C., & Berry, J. A. (1991). Physiological and environmental
720   regulation of stomatal conductance, photosynthesis and transpiration: a model that includes
721   a laminar boundary layer. *Agricultural and Forest Meteorology*, *54*(2), 107–136.
722   https://doi.org/10.1016/0168-1923(91)90002-8

723 Collatz, G. J., Ribas-Carbo, M., & Berry, J. (1992). Coupled Photosynthesis-Stomatal
724   Conductance Model for Leaves of C4 Plants. *Functional Plant Biology*, *19*(5), 519–538.
725   https://doi.org/10.1071/pp9920519

726 Davies-Barnard, T., & Friedlingstein, P. (2020). The Global Distribution of Biological Nitrogen
727   Fixation in Terrestrial Natural Ecosystems. *Global Biogeochemical Cycles*, *34*(3), 1–17.
728   https://doi.org/10.1029/2019GB006387

729 Davies-Barnard, T., Meyerholt, J., Zaehle, S., Friedlingstein, P., Brovkin, V., Fan, Y., et al.
730   (2020). Nitrogen cycling in CMIP6 land surface models: Progress and limitations.
731   *Biogeosciences*, *17*(20), 5129–5148. https://doi.org/10.5194/bg-17-5129-2020

732 Du, E., Terrer, C., Pellegrini, A. F. A., Ahlstrom, A., van Lissa, C. J., Zhao, X., et al. (2020).
733   Global patterns of terrestrial nitrogen and phosphorus limitation. *Nature Geoscience*, *13*(3),
734   221–226. https://doi.org/10.1038/s41561-019-0530-4

735 Elbert, W., Weber, B., Burrows, S., Steinkamp, J., Büdel, B., Andreae, M. O., & Pöschl, U.
736   (2012). Contribution of cryptogamic covers to the global cycles of carbon and nitrogen.
737   *Nature Geoscience*, *5*(7), 459–462. https://doi.org/10.1038/ngeo1486

738 Elser, J. J., Bracken, M. E. S., Cleland, E. E., Gruner, D. S., Harpole, W. S., Hillebrand, H., et al.
739   (2007). Global analysis of nitrogen and phosphorus limitation of primary producers in
740   freshwater, marine and terrestrial ecosystems. *Ecology Letters*, *10*(12), 1135–1142.
741   https://doi.org/10.1111/j.1461-0248.2007.01113.x

742 Elser, J. J., Fagan, W. F., Kerkhoff, A. J., Swenson, N. G., & Enquist, B. J. (2010). Biological
743   stoichiometry of plant production: Metabolism, scaling and ecological response to global
744   change. *New Phytologist*, *186*(3), 593–608. https://doi.org/10.1111/j.1469-
745   8137.2010.03214.x

746 Eyring, V., Bony, S., Meehl, G. A., Senior, C. A., Stevens, B., Stouffer, R. J., & Taylor, K. E.

747   (2016). Overview of the Coupled Model Intercomparison Project Phase 6 (CMIP6)
748   experimental design and organization. *Geoscientific Model Development*, *9*(5), 1937–1958.
749   https://doi.org/10.5194/gmd-9-1937-2016

750 Farquhar, G. D., von Caemmerer, S., & Berry, J. A. (1980). A biochemical model of
751   photosynthetic CO2 assimilation in leaves of C3 species. *Planta*, *149*(1), 78–90.
752   https://doi.org/10.1007/BF00386231

753 Finzi, A. C., Abramoff, R. Z., Spiller, K. S., Brzostek, E. R., Darby, B. A., Kramer, M. A., &
754   Phillips, R. P. (2015). Rhizosphere processes are quantitatively important components of
755   terrestrial carbon and nutrient cycles. *Global Change Biology*, *21*(5), 2082–2094.
756   https://doi.org/10.1111/gcb.12816

757 Fowler, D., Coyle, M., Skiba, U., Sutton, M. A., Cape, J. N., Reis, S., et al. (2013). The global
758   nitrogen cycle in the twenty-first century. *Philosophical Transactions of the Royal Society*
759   *B: Biological Sciences*, *368*(1621), 20130164. https://doi.org/10.1098/rstb.2013.0164

760 Friedlingstein, P., Jones, M. W., O'Sullivan, M., Andrew, R. M., Hauck, J., Peters, G. P., et al.
761   (2019). Global Carbon Budget 2019. *Earth System Science Data*, *11*(4), 1783–1838.
762   https://doi.org/10.5194/essd-11-1783-2019

763 Haverd, V., Smith, B., Nieradzik, L., Briggs, P. R., Woodgate, W., Trudinger, C. M., et al.
764   (2018). A new version of the CABLE land surface model (Subversion revision r4601)
765   incorporating land use and land cover change, woody vegetation demography, and a novel
766   optimisation-based approach to plant coordination of photosynthesis. *Geoscientific Model*
767   *Development*, *11*(7), 2995–3026. https://doi.org/10.5194/gmd-11-2995-2018

768 Hedin, L. O., Brookshire, E. N. J., Menge, D. N. L., & Barron, A. R. (2009). The Nitrogen
769   Paradox in Tropical Forest Ecosystems. *Annual Review of Ecology, Evolution, and*
770   *Systematics*, *40*(1), 613–635. https://doi.org/10.1146/annurev.ecolsys.37.091305.110246

771 Hengl, T., De Jesus, J. M., Heuvelink, G. B. M., Gonzalez, M. R., Kilibarda, M., Blagotić, A., et
772   al. (2017). SoilGrids250m: Global gridded soil information based on machine learning.
773   *PLoS ONE*, *12*(2), e0169748. https://doi.org/10.1371/journal.pone.0169748

774 Herridge, D. F., Peoples, M. B., & Boddey, R. M. (2008). Global inputs of biological nitrogen
775   fixation in agricultural systems. *Plant and Soil*, *311*(1), 1–18.
776   https://doi.org/10.1007/s11104-008-9668-3

777 Houlton, B. Z., Wang, Y. P., Vitousek, P. M., & Field, C. B. (2008). A unifying framework for
778   dinitrogen fixation in the terrestrial biosphere. *Nature*, *454*(7202), 327–330.
779   https://doi.org/10.1038/nature07028

780 Kattge, J., Knorr, W., Raddatz, T., & Wirth, C. (2009). Quantifying photosynthetic capacity and
781   its relationship to leaf nitrogen content for global-scale terrestrial biosphere models. *Global*
782   *Change Biology*, *15*(4), 976–991. https://doi.org/10.1111/j.1365-2486.2008.01744.x

783 Kerkhoff, A. J., Fagan, W. F., Elser, J. J., & Enquist, B. J. (2006). Phylogenetic and growth form

784   variation in the scaling of nitrogen and phosphorus in the seed plants. *The American*
785   *Naturalist*, *168*(4), E103–E122. https://doi.org/10.1086/507879

786   Köchy, M., Hiederer, R., & Freibauer, A. (2015). Global distribution of soil organic carbon –
787   Part 1: Masses and frequency distributions of SOC stocks for the tropics, permafrost
788   regions, wetlands, and the world. *Soil*, *1*(1), 351–365. https://doi.org/10.5194/soil-1-351-
789   2015

790   Kou-Giesbrecht, S., Malyshev, S., Martínez Cano, I., Pacala, S. W., Shevliakova, E.,
791   Bytnerowicz, T. A., & Menge, D. N. L. (2021). A novel representation of biological
792   nitrogen fixation and competitive dynamics between nitrogen-fixing and non-fixing plants
793   in a land model (GFDL LM4.1-BNF). *Biogeosciences*, *18*(13), 4143–4183.
794   https://doi.org/10.5194/bg-18-4143-2021

795   Koven, C., Arora, V., Cadule, P., Fisher, R., Jones, C., Lawrence, D., et al. (2021). 23rd Century
796   surprises: Long-term dynamics of the climate and carbon cycle under both high and net
797   negative emissions scenarios. *Earth System Dynamics Discussions*, (April), 1–32.
798   https://doi.org/10.5194/esd-2021-23

799   Lau, W. K. M., Wu, H. T., & Kim, K. M. (2013). A canonical response of precipitation
800   characteristics to global warming from CMIP5 models. *Geophysical Research Letters*,
801   *40*(12), 3163–3169. https://doi.org/10.1002/grl.50420

802   Lawrence, D. M., Fisher, R. A., Koven, C. D., Oleson, K. W., Swenson, S. C., Bonan, G., et al.
803   (2019). The Community Land Model Version 5: Description of New Features,
804   Benchmarking, and Impact of Forcing Uncertainty. *Journal of Advances in Modeling Earth*
805   *Systems*, *11*(12), 4245–4287. https://doi.org/10.1029/2018MS001583

806   LeBauer, D. S., & Treseder, K. K. (2008). Nitrogen Limitation of Net Primary Productivity in
807   Terrestrial Ecosystems is Globally Distributed. *Ecology*, *89*(2), 371–379.
808   https://doi.org/10.1016/j.agee.2013.04.020

809   Liang, J., Qi, X., Souza, L., & Luo, Y. (2016). Processes regulating progressive nitrogen
810   limitation under elevated carbon dioxide: A meta-analysis. *Biogeosciences*, *13*(9), 2689–
811   2699. https://doi.org/10.5194/bg-13-2689-2016

812   Liddicoat, S. K., Wiltshire, A. J., Jones, C. D., Arora, V. K., Brovkin, V., Cadule, P., et al.
813   (2021). Compatible fossil fuel CO_2 emissions in the CMIP6 earth system models' historical
814   and shared socioeconomic pathway experiments of the twenty-first century. *Journal of*
815   *Climate*, *34*(8), 2853–2875. https://doi.org/10.1175/JCLI-D-19-0991.1

816   Long, S. P. (1991). Modification of the response of photosynthetic productivity to rising
817   temperature by atmospheric CO2 concentrations: Has its importance been underestimated?
818   *Plant, Cell & Environment*, *14*(8), 729–739. https://doi.org/10.1111/j.1365-
819   3040.1991.tb01439.x

820   Luo, Y., Su, B., Currie, W. S., Dukes, J. S., Finzi, A., Hartwig, U., et al. (2004). Progressive
821   Nitrogen Limitation of Ecosystem Responses to Rising Atmospheric Carbon Dioxide.

822   *BioScience*, *54*(8), 731–739. https://doi.org/10.1641/0006-
823   3568(2004)054[0731:PNLOER]2.0.CO;2

824 Martens, B., Miralles, D. G., Lievens, H., Van Der Schalie, R., De Jeu, R. A. M., Fernández-
825   Prieto, D., et al. (2017). GLEAM v3: Satellite-based land evaporation and root-zone soil
826   moisture. *Geoscientific Model Development*, *10*(5), 1903–1925.
827   https://doi.org/10.5194/gmd-10-1903-2017

828 McGroddy, M. E., Daufresne, T., & Hedin, L. O. (2004). Scaling of C:N:P stoichiometry in
829   forests worldwide: Implications of terrestrial redfield-type ratios. *Ecology*, *85*(9), 2390–
830   2401. https://doi.org/10.1890/03-0351

831 Melton, J. R., Shrestha, R. K., & Arora, V. K. (2015). The influence of soils on heterotrophic
832   respiration exerts a strong control on net ecosystem productivity in seasonally dry
833   Amazonian forests. *Biogeosciences*, *12*(4), 1151–1168. https://doi.org/10.5194/bg-12-1151-
834   2015

835 Melton, J. R., Arora, V. K., Wisernig-Cojoc, E., Seiler, C., Fortier, M., Chan, E., & Teckentrup,
836   L. (2020). CLASSIC v1.0: The open-source community successor to the Canadian Land
837   Surface Scheme (CLASS) and the Canadian Terrestrial Ecosystem Model (CTEM)-Part 1:
838   Model framework and site-level performance. *Geoscientific Model Development*, *13*(6),
839   2825–2850. https://doi.org/10.5194/gmd-13-2825-2020

840 Menge, D. N. L., Wolf, A. A., & Funk, J. L. (2015). Diversity of nitrogen fixation strategies in
841   Mediterranean legumes. *Nature Plants*, *1*(6), 1–5. https://doi.org/10.1038/nplants.2015.64

842 Meyerholt, J., & Zaehle, S. (2015). The role of stoichiometric flexibility in modelling forest
843   ecosystem responses to nitrogen fertilization. *New Phytologist*, *208*(4), 1042–1055.
844   https://doi.org/10.1111/nph.13547

845 Meyerholt, J., Sickel, K., & Zaehle, S. (2020). Ensemble projections elucidate effects of
846   uncertainty in terrestrial nitrogen limitation on future carbon uptake. *Global Change*
847   *Biology*, *26*(7), 3978–3996. https://doi.org/10.1111/gcb.15114

848 Minchin, F. R., & Witty, J. F. (2005). Respiratory/Carbon Costs of Symbiotic Nitrogen Fixation
849   in Legumes. In *Plant Respiration* (pp. 195–205). Dordrecht: Springer.
850   https://doi.org/10.1007/1-4020-3589-6_11

851 O'Hara, G. W. (1998). The role of nitrogen fixation in crop production. *Journal of Crop*
852   *Production*, *1*(2), 115–138. https://doi.org/10.1201/9780203745281

853 Peng, J., Wang, Y. P., Houlton, B. Z., Dan, L., Pak, B., & Tang, X. (2020). Global Carbon
854   Sequestration Is Highly Sensitive to Model-Based Formulations of Nitrogen Fixation.
855   *Global Biogeochemical Cycles*, *34*(1), e2019GB006296.
856   https://doi.org/10.1029/2019GB006296

857 Phillips, R. P., Brzostek, E., & Midgley, M. G. (2013). The mycorrhizal-associated nutrient
858   economy: A new framework for predicting carbon-nutrient couplings in temperate forests.

859   *New Phytologist*, *199*(1), 41–51. https://doi.org/10.1111/nph.12221

860   Le Quéré, C., Andrew, R. M., Friedlingstein, P., Sitch, S., Pongratz, J., Manning, A. C., et al.
861   (2018). Global Carbon Budget 2018. *Earth System Science Data*, *10*(4), 2141–2194.
862   https://doi.org/10.5194/essd-2017-123

863   Reed, S. C., Cleveland, C. C., & Townsend, A. R. (2011). Functional Ecology of Free-Living
864   Nitrogen Fixation: A Contemporary Perspective. *Annual Review of Ecology, Evolution, and*
865   *Systematics*, *42*(1), 489–512. https://doi.org/10.1146/annurev-ecolsys-102710-145034

866   Seiler, C., Melton, J., Arora, V., & Wang, L. (2021). CLASSIC v1.0: the open-source
867   community successor to the Canadian Land Surface Scheme (CLASS) and the Canadian
868   Terrestrial Ecosystem Model (CTEM) – Part 2: Global Benchmarking. *Geoscientific Model*
869   *Development*, *14*(5), 2371–2417. https://doi.org/10.5194/gmd-2020-294

870   Sistla, S. A., & Schimel, J. P. (2012). Stoichiometric flexibility as a regulator of carbon and
871   nutrient cycling in terrestrial ecosystems under change. *New Phytologist*, *196*(1), 68–78.
872   https://doi.org/10.1111/j.1469-8137.2012.04234.x

873   Song, J., Wan, S., Piao, S., Knapp, A. K., Classen, A. T., Vicca, S., et al. (2019). A meta-analysis
874   of 1,119 manipulative experiments on terrestrial carbon-cycling responses to global change.
875   *Nature Ecology and Evolution*, *3*(9), 1309–1320. https://doi.org/10.1038/s41559-019-0958-
876   3

877   Stocker, B. D., Prentice, I. C., Cornell, S. E., Davies-Barnard, T., Finzi, A. C., Franklin, O., et al.
878   (2016). Terrestrial nitrogen cycling in Earth system models revisited. *New Phytologist*,
879   *210*(4), 1165–1168. https://doi.org/10.1111/nph.13997

880   Sullivan, B. W., Alvarez-Clare, S., Castle, S. C., Porder, S., Reed, S. C., Schreeg, L., et al.
881   (2014). Assessing nutrient limitation in complex forested ecosystems: Alternatives to large-
882   scale fertilization experiments. *Ecology*, *95*(3), 668–681. https://doi.org/10.1890/13-0825.1

883   Sulman, B. N., Shevliakova, E., Brzostek, E. R., Kivlin, S. N., Malyshev, S., Menge, D. N. L., &
884   Zhang, X. (2019). Diverse mycorrhizal associations enhance terrestrial C storage in a global
885   model. *Global Biogeochemical Cycles*, *33*(4), 501–523.
886   https://doi.org/10.1029/2018GB005973

887   Swart, N. C., Cole, J. N. S., Kharin, V. V, Lazare, M., Scinocca, J. F., Gillett, N. P., et al. (2019).
888   The Canadian Earth System Model version 5 (CanESM5.0.3). *Geoscientific Model*
889   *Development*, *12*(11), 4823–4873. https://doi.org/10.5194/gmd-12-4823-2019

890   Terrer, C., Vicca, S., Stocker, B. D., Hungate, B. A., Phillips, R. P., Reich, P. B., et al. (2018).
891   Ecosystem responses to elevated CO_2 governed by plant-soil interactions and the cost of
892   nitrogen acquisition. *New Phytologist*, *217*(2), 507–522. https://doi.org/10.1111/nph.14872

893   Terrer, C., Prentice, I., Jackson, R., Keenan, T., Kaiser, C., Vicca, S., et al. (2019). Nitrogen and
894   phosphorus constrain the CO_2 fertilization of global plant biomass. *Nature Climate Change*,
895   *9*(9), 684–689. https://doi.org/10.1038/s41558-019-0545-2

Thomas, R. Q., Brookshire, E. N. J., & Gerber, S. (2015). Nitrogen limitation on land: How can it occur in Earth system models? *Global Change Biology*, *21*(5), 1777–1793. https://doi.org/10.1111/gcb.12813

Verseghy, D. L. (1991). CLASS — A Canadian land surface scheme for GCMS. I. Soil model. *International Journal of Climatology*, *11*(2), 111–133.

Verseghy, D. L., McFarlane, N. A., & Lazare, M. (1993). CLASS — A Canadian land surface scheme for GCMS, II. Vegetation model and coupled runs. *International Journal of Climatology*, *13*(4), 347–370. https://doi.org/10.1002/joc.3370130402

Vitousek, P. M., Menge, D. N., Reed, S. C., & Cleveland, C. C. (2013). Biological nitrogen fixation: rates, patterns and ecological controls in terrestrial ecosystems. *Philosophical Transactions of the Royal Society B: Biological Sciences*, *368*(1621), 20130119. https://doi.org/10.1098/rstb.2013.0119

Walker, A. P., De Kauwe, M. G., Bastos, A., Belmecheri, S., Georgiou, K., Keeling, R. F., et al. (2020). Integrating the evidence for a terrestrial carbon sink caused by increasing atmospheric CO_2. *New Phytologist*, *229*(5), 2413–2445. https://doi.org/10.1111/nph.16866

Wang, Y. P., Law, R. M., & Pak, B. (2010). A global model of carbon, nitrogen and phosphorus cycles for the terrestrial biosphere. *Biogeosciences*, *7*(7), 2261–2282. https://doi.org/10.5194/bg-7-2261-2010

Weedon, J. T., Cornwell, W. K., Cornelissen, J. H. C., Zanne, A. E., Wirth, C., & Coomes, D. A. (2009). Global meta-analysis of wood decomposition rates: A role for trait variation among tree species? *Ecology Letters*, *12*(1), 45–56. https://doi.org/10.1111/j.1461-0248.2008.01259.x

Wieder, W. R., Cleveland, C. C., Lawrence, D. M., & Bonan, G. B. (2015). Effects of model structural uncertainty on carbon cycle projections: Biological nitrogen fixation as a case study. *Environmental Research Letters*, *10*(4), 044016. https://doi.org/10.1088/1748-9326/10/4/044016

Wright, S. J., Turner, B. L., Yavitt, J. B., Harms, K. E., Kaspari, M., Tanner, E. V. J., et al. (2018). Plant responses to fertilization experiments in lowland, species-rich, tropical forests. *Ecology*, *99*(5), 1129–1138. https://doi.org/10.1002/ecy.2193

Xu, L., Saatchi, S. S., Yang, Y., Yu, Y., Pongratz, J., Anthony Bloom, A., et al. (2021). Changes in global terrestrial live biomass over the 21st century. *Science Advances*, *7*(27), eabe9829. https://doi.org/10.1126/sciadv.abe9829

Yuan, Z. Y., Chen, H. Y. H., & Reich, P. B. (2011). Global-scale latitudinal patterns of plant fine-root nitrogen and phosphorus. *Nature Communications*, *2*(1), 1–6. https://doi.org/10.1038/ncomms1346

Zheng, M., Zhou, Z., Luo, Y., Zhao, P., & Mo, J. (2019). Global pattern and controls of biological nitrogen fixation under nutrient enrichment: A meta-analysis. *Global Change*

933   *Biology*, *25*(9), 3018–3030. https://doi.org/10.1111/gcb.14705

934   Zheng, M., Zhou, Z., Zhao, P., Luo, Y., Ye, Q., Zhang, K., et al. (2020). Effects of human
935   disturbance activities and environmental change factors on terrestrial nitrogen fixation.
936   *Global Change Biology*, *26*(11), 6203–6217. https://doi.org/10.1111/gcb.15328

937   Zhu, Q., Riley, W. J., Tang, J., Collier, N., Hoffman, F. M., Yang, X., & Bisht, G. (2019).
938   Representing Nitrogen, Phosphorus, and Carbon Interactions in the E3SM Land Model:
939   Development and Global Benchmarking. *Journal of Advances in Modeling Earth Systems*,
940   *11*(7), 2238–2258. https://doi.org/10.1029/2018MS001571

941